Development of Functional Electrodes toward Efficient Electrochemical Catalytic Redox Reactions of Oxygen/Water under Neutral Conditions and Ambient Temperature

TAKAAKI NAKAGAWA

Doctoral Program in Materials Science

Submitted to the Graduate School of

Pure and Applied Sciences

in Partial Fulfillment of the Requirements

for the Degree of Doctor of Philosophy in

Engineering

at the

University of Tsukuba

Contents

1. General introduction

1.1. Electrochemical oxygen reduction and water oxidation at ambient temperature and neutral pH

1.1.1. Electrochemical reactions with large overpotentials

The exhaustion of the earth's finite supply of fossil fuels and other natural resources is a global problem owing to a rapid increase in population in recent decades. Conversely, the essentially infinite light energy radiating from the sun is converted in nature into carbohydrates such as glucose via photosynthesis; using water and carbon dioxide as feedstocks, light energy is converted into chemical energy. Animals can then convert the carbohydrates back into water and carbon dioxide using the oxygen in their respiratory system, regenerating the starting materials and completing an energy cycle (Figure 1.1). Both processes occur at neutral pH and ambient temperatures, in spite of complicated reaction pathways consisting of several reaction steps. A great deal of scientific research has been devoted to such reactions and their catalysts in order to mimic these functions in processes such as artificial photosynthesis and biofuel cells; the former system converts light energy to chemical energy, the latter system converts chemical energy into electrical energy.
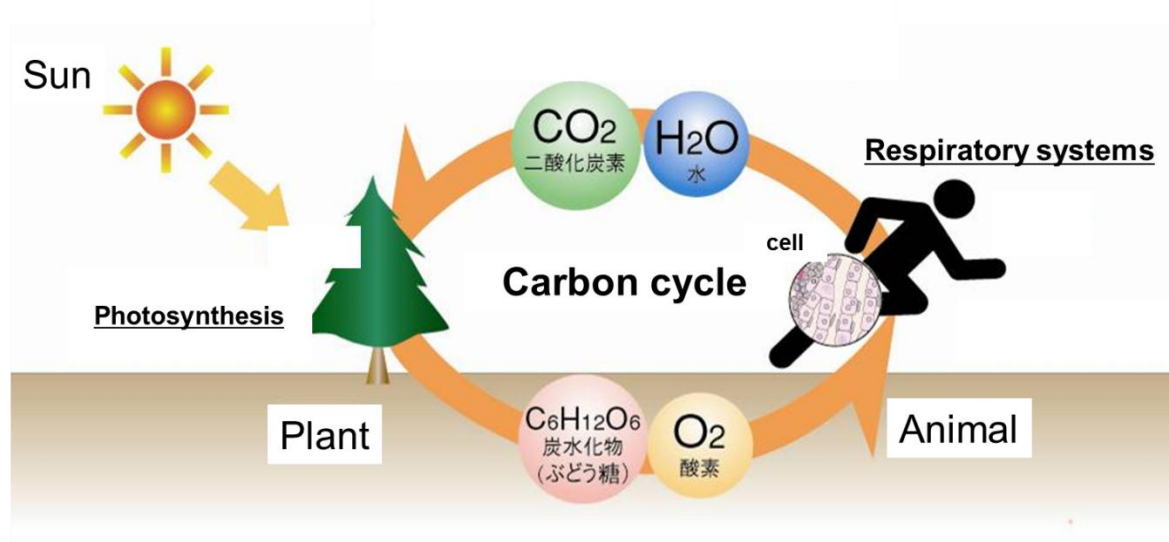
Figure 1.1. Energy and carbon circle systems of nature[1]

・Artificial photosynthesis:

$$2 H_2O \rightarrow O_2 + 4 H^+ + 4 e^-$$

$$4 H^+ + 4 e^- \rightarrow 2 H_2$$

Overall reaction: $\quad 2 H_2O \rightarrow 2 H_2 + O_2$

・Biofuel cell:

$$C_6H_{12}O_6 + 6 H_2O \rightarrow 6 CO_2 + 24 H^+ + 24 e^-$$

$$6 O_2 + 24 H^+ + 24 e^- \rightarrow 12 H_2O$$

Overall reaction: $\quad C_6H_{12}O_6 + 6 O_2 \rightarrow 6 CO_2 + 6 H_2O$
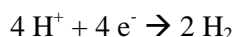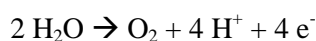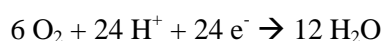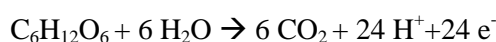
Scheme 1.1. Chemical reactions in artificial photosynthesis and biofuel cells.

Water is oxidized to oxygen in artificial photosynthesis, while oxygen is reduced to water in biofuel cells. Numerous problems exist from the perspective of the practical application of such reactions, such as efficiency, stability, cost issues, and usability. It is particularly important to discover novel catalysts for such reactions and develop electrodes with suitable structures that maximize the expected effects from catalysts in order to improve their efficiency.

The realization of such energy conversion systems under conditions such as neutral pH, room temperature, and atmospheric pressure potentially brings great advantages such as the safety and simplification of the system. However, it is difficult to efficiently promote artificial photosynthesis and biofuel cell reactions under mild conditions. In general, the redox reactions of electrochemically reversible materials such as electron mediators occur at their formal redox potential, such that a catalyst is not needed. However, oxygen and water are electrochemically irreversible materials; the formal redox potential of water/oxygen is 0.62 V vs. Ag|AgCl (sat.) at pH 7.0; however, the system requires more than 1.0 V against formal redox potentials (overpotential) without a catalyst in order for both reactions to proceed. An efficient electrochemical water/oxygen redox system is therefore needed in both applications because of its large overpotential against the formal redox potential of oxygen/water. Water is oxidized to oxygen in artificial

3

photosynthesis, whereas oxygen is reduced to water in biofuel cells by a suitable catalyst. In general, metal oxides or metal complexes are used in the former process, while metals or enzymes are used as catalysts in the latter.

1.1.2. Practical functional electrodes

Iridium oxide nanoparticles and bilirubin oxidase (BOD) have been employed as catalysts for water oxidation and oxygen reduction to water, respectively. Both catalysts are well known, however their catalytic activity is insufficient because of the strong dependence on how the catalyst is applied to the electrode surface. In general, such catalysts require immobilization on electrode surfaces for two reasons: to prevent their leaching into the electrolyte solution, and to improve electron transfer between the catalyst and the electrode during practical use. However, electrodes that possess a high surface area with a modified catalyst and fast electron transfer are insufficient. In order to obtain adequate catalytic activity, it is essential to produce efficient functional electrodes by increasing the available electrode surface area, such that the ion concentration and mass transfer of protons, water, and oxygen is adequate around the catalyst. Furthermore, modified electrodes are efficient because it is not necessary to regenerate any compounds attached to the electrode—such as the catalyst—when replenishing the apparatus during practical use. In such systems, efficient electrochemical redox reactions of water/oxygen are achieved at neutral pH, room temperature, and atmospheric pressure by the development of efficient, functional electrodes which are compatible with such conditions.

1.2. Introduction to the electrochemical reduction of oxygen to water in biofuel cells

1.2.1. Biofuel cells

Biofuel cells are next generation energy devices that generate electricity from renewable fuels such as sugars, alcohols, and organic acids through the use of enzymes or microorganisms as a catalyst.[2-6] They are classified according to the type of the catalyst which is enzyme or microorganisms in a anode. Moreover, they are also classified whether electron mediator is needed or not (Figure 1.2). Some suitable electrocatalysts are required to generate electricity for the oxidation of organic materials in bioanodes. Conventional metal catalysts such as gold or silver nanoparticles only function in strongly basic conditions.[7] In order to operate at neutral pH and at room temperature, enzymes such as glucose oxidase, glucose dehydrogenase, and alcohol dehydrogenase are used as electrocatalysts. Biocathode catalysts also function under similar conditions. The theoretical redox potentials of the bioanodic reaction and biocathodic reaction are –0.43 V and 0.82 V vs. the standard hydrogen electrode (SHE), respectively, yielding a theoretical biofuel cell voltage of 1.25 V.
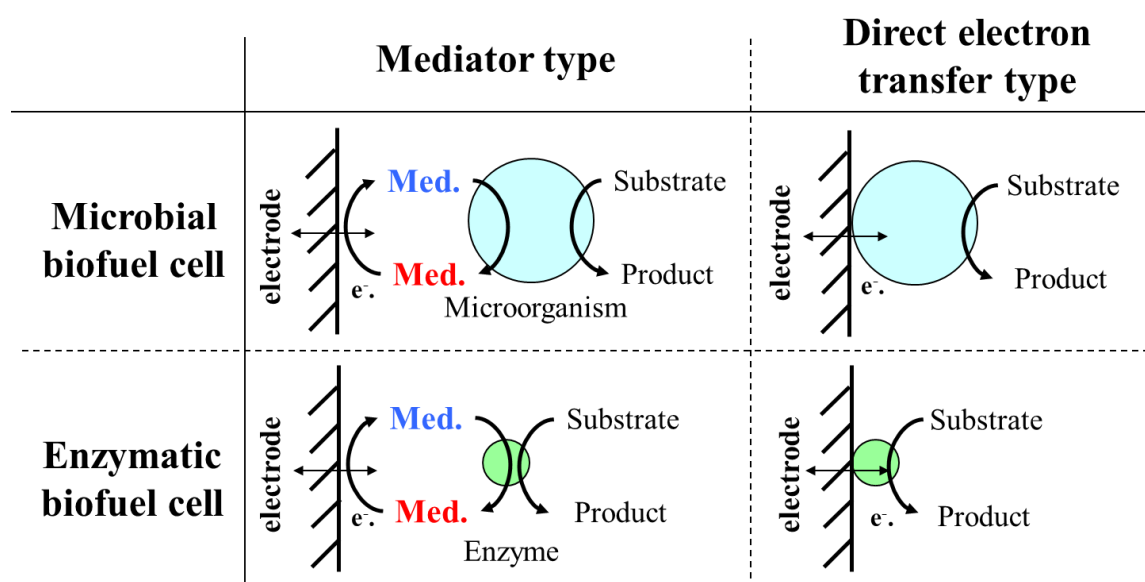
Figure 1.2. Types of biofuel cells. Med. shows electron mediator.

The energy capacity of the biofuel cell (using glucose as a fuel) is calculated from:

$$\Delta G^{o} (= -nFE^{o}) \qquad (1.1)$$

where ΔG^{o} is the Gibbs free energy, n is the number of electrons, F is the Faraday constant, and E^{o} is the

electrode potential)

The value of ΔG^{o} was determined as **-2872 kJ/mol**, giving a theoretical capacity of 4.4 Wh/g glucose,

which is about 10 times higher than that of a conventional rechargeable Li-ion battery. In order to realize this

high capacity, it is important to reduce the overpotential of both the cathode and anode reactions.

1.2.2. Cathodic biocatalysts

In general, platinum is an excellent catalyst for the reduction of oxygen in strongly acidic conditions

and has been already applied in commercial fuel cells containing methanol and hydrogen. However, the

platinum catalyst requires a large overpotential to accelerate the reaction at neutral pH; at overpotentials of

less than 1 V, oxygen is reduced to peroxidase rather than water. In order to accomplish the reduction of

oxygen to water in weakly acidic conditions and at ambient temperature with low overpotentials,

multi-copper oxidases such as fungal laccase (EC 1.10.3.2) and ascorbate oxidase are useful as catalysts.[8-9]

Tsujimura *et al.* have reported that the multi-copper oxidase BOD from *Myrothecium verrucaria*, (EC

1.3.3.5) reduces oxygen to water at pH 7 and ambient temperature.[10] BOD which molecular mass is 60 kDa

can oxidase bilirubin to biliverdin with reduction of oxygen to water.[11] There are at least four Cu atoms that

are classified based on their properties; at least one Type 1, one Type 2, and two Type 3 Cu atoms. The Type

1 Cu is located adjacent to the binding site of the electron donor and has a role in electron transfer from the

substrate to the oxygen- reduction site of the enzyme, known as the ''tri-nuclear cluster''.[12] These enzyme

catalysts are ideally lower cost compared to precious rare metal catalyst on the basis of catalytic activity per

unit volume.[13]

1.2.3. Enzyme-modified cathodes based on redox mediators

The modification of electrodes using enzymes as catalysts incurs problems not found in similar processes involving metal catalysts. In general, enzymes cannot directly transport electrons to the electrode because the active site is located deep within its interior; an electron mediator is required to be immobilized on electrode with the enzyme, while retaining the enzyme's activity. Figure 1.3 shows the conventional mediator type glucose biofuel cell. The actual cell voltage is determined by a difference between a potential of mediator at cathode and at anode. Ideal electron mediators for biofuel cells possess features which include the ability to transfer electrons between the enzyme and the electrode, a potential close to the redox potential

anode
$C_6H_{12}O_6 + 6H_2O \rightarrow 6CO_2 + 24H^+ + 24e^-$

separator

cathode
$O_2 + 4H^+ + 4e^- \rightarrow 2H_2O$
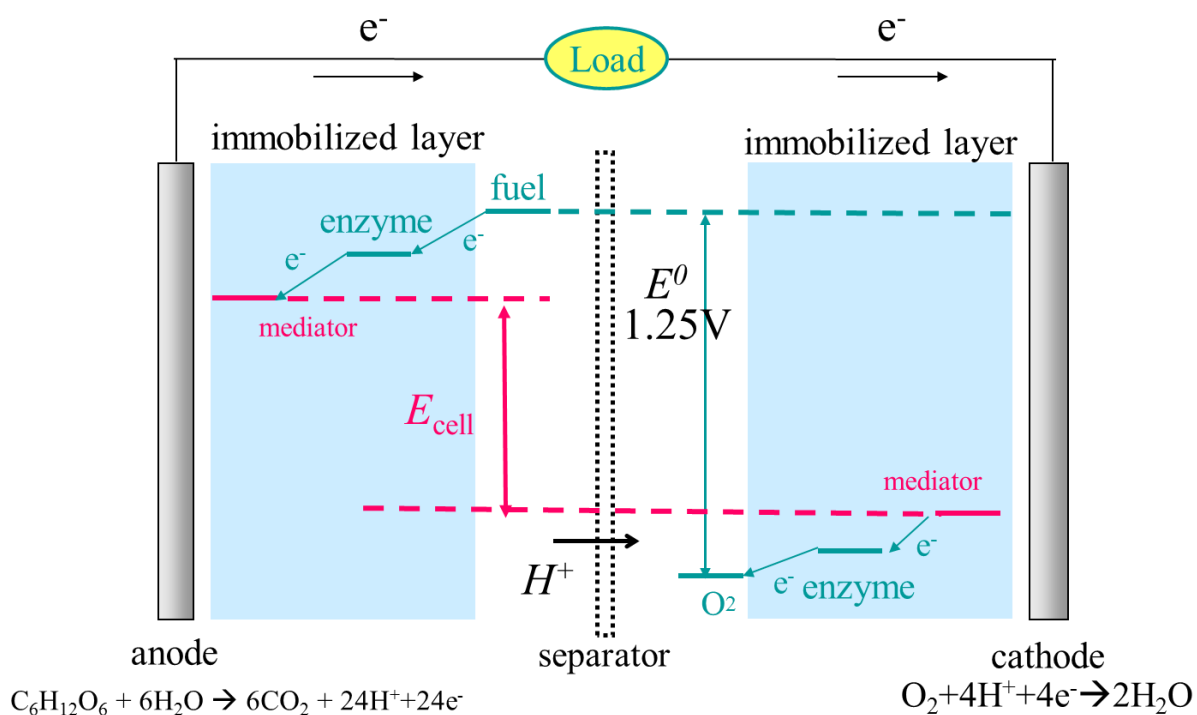
Figure 1.3. Structure of mediator type glucose biofuel cell

of oxygen/water (in order to increase the cell voltage and energy conversion efficiency), and chemical stability. For example, 2,2'-azino-bis(3-ethylbenzothiazoline-6-sulphonic acid) (ABTS) and its osmium complex is well known as a redox mediator between laccase and BOD. ABTS is a good mediator due to its affinity for BOD (as demonstrated by turnover frequency (k_{cat}) and Michaelis constant for mediator (K_M) values) and its potential, however its low stability is a problem. The osmium complex can be synthesized

with several potentials, but its application is impractical as osmium is more expensive than platinum.

1.2.4. Enzyme immobilization

It is well known that cross-linkers such as glutaraldehyde strongly bind modified enzymes on electrode surfaces, but the loss of enzyme activity is sometimes significant. Semipermeable membranes can also separate enzyme solutions from bulk solutions. Both methods are, however, unsuitable for modified electron mediators in this context because they are much smaller in scale than macromolecules such as enzymes. Heller *et al.* reported a modified method that cross-linked an osmium complex (as the electron mediator) and enzyme via poly(ethy1ene glycol) diglycidyl ether onto a graphite electrode; the electrocatalyst was a composite of laccase cross-linked with a redox polymer on a hydrophilic cloth comprised of 10 μm diameter carbon fibers. The redox polymer, PVI−Os(tpy)(dme-bpy)$^{2+/3+}$ (PVI = poly-N-vinyl imidazole with 20% of the imidazoles bound to [Os(tpy)(dme-bpy)]$^{2+/3+}$ (tpy = terpyridine, dme-bpy = 4,4'-dimethyl-2,2'-bipyridine)), electronically connects the laccase reaction centers to the fibers.[14] This method is only useful when the cross-linker can replace ligands in the mediator complex, and it is difficult to apply this modification method to conventional electron mediators. In addition to the reasons discussed in previous sections, the immobilization of the enzyme and mediator is a significant consideration when fabricating functional electrodes which can efficiently reduce oxygen to water.

1.2.5. Increasing the electrode surface area

Porous electrodes are useful for increasing the catalytic current density per unit of electrode surface area. It is well known that mesoporous electrodes composed of mixtures of carbon powder and polymer (such as polytetrafluoroethylene (PTFE) or Nafion$^{®}$) as a binding agent are useful cathodes for fuel cells because of the large electrode surface area. However, it is very difficult to modify the electrodes with enzymes because such carbon/polymer composites are unstable towards hydrophobic materials and acidic solutions. However, such reactivity is advantageous: carbon fiber electrodes are suitable precursors to

enzyme-modified electrodes because the enzyme/mediator solution easily soaks into the structure of the porous electrode. Carbon fiber electrodes modified with enzymes and mediators can easily form annuli by using rotating disk electrode (RDE) systems because such electrodes are sufficiently pliant to be manipulated by this technique.(Figure 1.4)
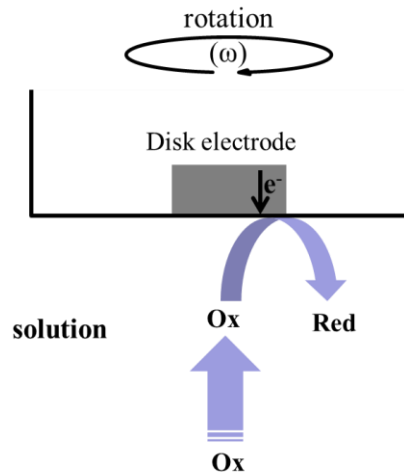
Figure 1.4. Image of mass transfer flow at rotating disk electrode system

1.2.6. Evaluation of oxygen-reduction electrodes

Functionalized electrodes which contain modified catalysts and other components can be analyzed by electrochemical measurements using the three electrode method. The catalytic current is determined by a limiting step of either catalytic activity or substrate/proton mass transfer. However, the solubility of oxygen in water is only 0.25 mM in air-saturated conditions or 1.25 mM in oxygen-saturated conditions. RDE systems are useful in order to supply enough substrate to maintain catalytic activity. In the RDE system (Figure 1.4), oxygen and protons are supplied with rotating speed. The current is determined by the Levich equation:

$$i_{mass} = 0.62nFAD^{2/3}v^{-1/6}\omega^{1/2}C \qquad (1.2)$$

where i_{mass} is the limiting current, n is the number of electrons, F is the Faraday constant, A is the electrode surface area, D is the diffusion coefficient, v is the viscosity, ω is the speed of rotation, and C is the limiting current. If the catalytic activity of the functional electrode is sufficient, the current increases linearly

with the square root of the rotating rate.

The limiting catalytic current of the functional electrode is determined when the catalytic current is saturated, while the rotation speed is increased. Using the equation shown below, plotting $1/i_{lim}$ vs. $1/\omega^{1/2}$ yields a plot whose y-intercept is the inverse of the limiting current, as determined by the kinetic constant (i_k):

$$1/i_{\mathrm{lim}} = 1/i_{\mathrm{k}} + 1/i_{\mathrm{mass}} \qquad (1.3)$$

The kinetic constant can be calculated using the equation:

$$i_k = n\,F\,A\,k\,\Gamma \qquad (1.4)$$

where k is the kinetic constant for the enzyme catalyst and Γ is the surface catalyst concentration.

1.3. Introduction to the electrochemical oxidation of water to oxygen

1.3.1. Photoelectrodes

Photocatalytic water splitting uses light energy to drive the thermodynamically uphill conversion of water into its constituent elements. Fujishima and Honda reported the first example of water splitting with TiO_2 photoelectrodes under UV illumination in 1972,[15] and much effort has been applied to the development of photosystems for the cleavage of water into H_2 and O_2 by visible light.[16-19] Although the reaction is thermodynamically possible with light at a wavelength of 1000 nm, efficient water photolysis has not yet been reported. Highly efficient photostable sensitizers which trap light photons and convert them into chemical energy are required in artificial photosynthesis, in addition to electrochemical catalysts which can split water into oxygen and hydrogen. One of the key components of such photolysis systems is a catalyst that converts water into O_2.[20-24] As a four-electron redox process involving two molecules of water, the evolution of O_2 from water is more challenging than kinetically simpler processes such as H_2 evolution.

1.3.2. Catalysts for the water oxidation reaction

A catalyst which evolves O_2 in water oxidation is necessary for the anode in numerous industrial electrochemical processes[25] such as the electrolysis of water, electroplating, electrosynthesis, and electrowinning, as well as in artificial photosynthetic devices which provide renewable energy.[26] Certain metal complexes—Ir and Ru in particular—[27-40] raised to high oxidation states are known catalysts for water oxidation. High-valent metal oxides including RuO_2, IrO_2, Co_3O_4, Rh_2O_3, and Mn_2O_3 also show activity as water oxidation catalysts.[22-24,31,32-33] Harriman[22-24] and co-workers demonstrated that high-valent states of citrate-stabilized IrO_2 particles actively oxidize water. Nocera[34] has reported that films containing Co^{2+} and phosphate deposited onto indium tin oxide (ITO) electrodes electrochemically oxidize water at pH 7. Using a different approach, Mallouk[31] successfully used electron transfer to adsorbed, photogenerated $[Ru(bpy)_3]^{3+}$ to

oxidatively charge 2 nm butylmalonate-stabilized IrO_2 nanoparticles. Yagi[33] showed that 50–100 nm diameter citrate-stabilized IrO_2 nanoparticles spontaneously adsorb on ITO electrodes; about 16% of the Ir sites in the resulting films are active water oxidation catalysts, although only 3.7 % of the IrO_2 is electrochemically active in the planar IrO_2 electrodes.[35] Nanoparticle size is strongly related to catalyst efficiency because the active surface area of the catalyst increases markedly, although it is difficult to prevent small nanoparticles aggregating with each other. It is well-known that tricarboxylic acid and dicarboxylic acid ligands are strong ligands to stabilize IrO_2 nanoparticles, however such nanoparticles can transfer electrons to an indium tin oxide (ITO) electrode surface only when adsorbed because of the chemical interaction between the carboxylic groups on the citrate stabilizer and hydroxyl groups on the ITO surface.[33] The catalytic current density increases to about 3 mA/cm^2 as the amount of adsorbed IrO_2 nanoparticles is increased. However, the catalytic current density does not increase beyond 3 mA/cm^2 despite the added IrO_2, due to slow electron transfer between nanoparticles and the low conductivity of nanoparticle films. Additionally, the electron transfer rate between conventional IrO_2 nanoparticles and carbon, gold, platinum, and ITO electrodes is typically slow when the nanoparticles are dissolved in solution. In order to achieve efficient functional electrodes, it is vital to improve electron transfer. In general, the electron transfer rate between an electrode and a nanoparticle is determined by ligand length and structure.[36] Moreover, it is expected that nanoparticles stabilized with short ligands can transfer electrons to each other so that electrons are transported quickly through the nanoparticle film.

1.3.3. Evaluation of water oxidation electrodes

In general, Clark's oxygen electrode is used to detect oxygen concentrations in electrochemical reactions. The change in oxygen concentration is continuously monitored by the oxygen electrode during the water oxidation reaction at the catalyst-modified electrode. This method is also used to monitor biological oxygen generation reactions (photosynthesis) and oxygen consumption reactions (respiration). The electrode has found a wide range of applications because of its simple experimental apparatus. Nocera *et al.* have

reported an alternative oxygen detection method using isotopically enriched ^{18}O; electrolysis was performed in helium-saturated electrolyte containing 14.6% [18]OH$_2$ in a gas-tight electrochemical cell. The cell was coupled to a mass spectrometer to confirm that water is the source of the O$_2$ produced. Helium carrier gas continuously flowed through the headspace of the anodic compartment into the mass spectrometer, and the relative abundances of [32]O$_2$, [34]O$_2$, and [36]O$_2$ were monitored at 2 s intervals. Within minutes of initiating electrolysis at 1.29 V, the signals for the three isotopes began to rise above background levels as the O$_2$ produced by the catalyst escaped into the headspace. However, both methods are unsuitable for the detection of very slight changes in oxygen concentration, because generated oxygen spreads through the solution and cell headspace. The oxygen level is central to understanding the overpotential at which water is oxidized to oxygen, therefore more accurate methods of monitoring low oxygen concentrations are required in such cases. Rotating ring disk electrode (RRDE) systems are suitable for oxygen detection purposes because oxygen generated by electrocatalytic reactions on the disk electrode is detected by a ring electrode which is positioned close to the disk electrode. (Figure 1.5) The collection efficiency N (the ratio of ring to disk current) is ~0.37, dependent on the RRDE structure (i.e., the surface area of each electrode, and the distance between them).
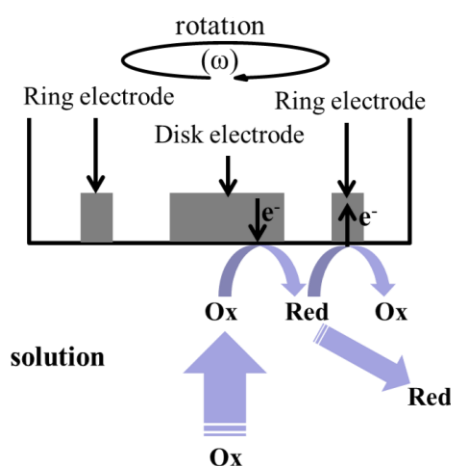
Figure 1.5. Image of mass transfer flow at at rotating ring disk electrode system.

$$N \ = \ |i_{Disk}| \, / \, |i_{Ring}| \qquad (1.5)$$

About 18.5% of oxygen generated from the disk electrode can be analyzed by the ring electrode, because the ratio between the numbers of electrons that reduce oxygen on the ring electrode, to that of electrons that oxidize water on the disk electrode is 1:2. The enhanced sensitivity of the RRDE system is suitable for the mechanistic investigation of electrode-oxidized water.

References and Notes

(1)   http://www.sony.co.jp/SonyInfo/technology/technology/theme/bio_01.html

(2)   Palmore, G.T.R.; Whitesides, G.M. Microbial and Enzymatic Biofuel Cells in Enzymatic Conversion of Biomass for Fuels Production, Vol. 566. (eds. M.E. Himmel, J.O. Baker & R.P. Overend) 271-290 (Amer Chemical Soc, Washington; 1994).

(3)   Ikeda, T.; Kano, K. *J. Biosci. Bioeng*. **2001**, 92, 9-18.

(4)   Barton, S.C.; Gallaway, J.; Atanassov, P. *Chem. Rev.* **2004,** 104, 4867-4886

(5)   Logan, B.E. *et al. Environ. Sci. Technol.* **2006***,* 40, 5181-5192.

(6)   Willner, I.; Yan, Y.M.; Willner, B.; Tel-Vered, R. *Fuel Cells* **2009,** 9, 7-24.

(7)   Tominaga, M.; Shimazoe, T.; Nagashima, M.; Kusuda, H.; Kubo, A.; Kuwahara, Y.; Taniguchi, I. *J. Electroanal. Chem.* **2006**, 590, 1, 37.

(8)   Palmore, G.T.R.; Kim, H-H. *J. Elctroanal. Chem.* **1999**, 461, 1, 110.

(9)   Mano, N.; Mao, F.; Heller, A. *J. Am. Chem. Soc.* **2002**, 124, 44, 12962.

(10)   Tsujimura, S.; Tatsumi, H.; Ogawa, J.; Shimizu, S.; Kano, K.; Ikeda, T. *J. Electroanal. Chem.* **2001**, 496, 69.

(11)   a) Cracknell, J. A.; McNamara, T. P.; Loweb, E. D.; Blanford, C. F. *Dalton Trans.* **2011**, 40, 6668. b) Cracknell, J. A.; Blanford, C. F. *Chem. Sci.* **2012**, 3, 1567.

(12)   a) Solomon, E. I.; Sundaram, U. M.; Machonkin, T. E. *Chem. Rev.* **1996**, 96, 2563–2605. b) Bertrand, T.; Jolivalt, C.; Briozzo, P.; Caminade, E.; Joly, N.; Madzak, C.; Mougin, C. *Biochemistry* **2002**, 41, 7325–7333.

(13)   Gasteiger, H. A.; Kocha, S. S.; Sompalli, B.; Wagner, F. T. *Appl. Catal.* **2005**, B, 56, 9 (2005).

(14)   Barton S.C.; Kim H-H.; Binyamin G.; Zhang Y.; Heller A. *J. Phys. Chem. B,* **2001**, 105 (47), 11917–11921

(15)   Fujishima, A.; Honda, K. *Nature* **1972**, 238, 37.

(16)   Domen, K. *Catal. Today*, **1998**, 44, 17.

(17)   Khaselev, O.; Turner, J.A. *Science*, **1998**, 280, 425.

(18)   Kudo, A.; Kato, H.; Nakagawa, S. *J. Phys. Chem. B*, **2000**, 104, 571.

(19)   Kim, H.G.; Hwang, D. W.; Kim, J.; Kim Y. G.; Lee, J. S. *Chem. Commun.* **1999**, 1077.

(20)   Kiwi, J.; Grätzel, M. *Nature*, **1979**, 285, 657.

(21)   Kiwi, J.; Grätzel, M. *J. Am. Chem. Soc.* **1979**, 101, 7214.

(22)   Harriman, A.; Richoux, M.; Christensen, P. A.; Moseri, S.; Neta, P. *J. Chem. Soc., Faraday Trans. 1*, **1987**, 83, 3001.

(23)   Harriman, A.; Thomas J. M.; Millward, G. R. *New J. Chem.* **1987**, 11, 757.

(24)   Harriman, A.; Pickering, I. J.; Thomas J. M.; Christensen, P. A. *J. Chem. Soc., Faraday Trans. 1*, **1988**, 84, 2795.

(25)   Chen, G.; Chen, X.; Yue, P.L. *J. Phys. Chem. B* **2002,** 106, 4364.

(26)   Yagi, M.; Kaneko, M. *Chem. Rev.* **2001**, 101, 21.

(27)   a) Gersten, S. W.; Samuels, G. J.; Meyer, T. J. *J. Am. Chem. Soc.* **1982**, 104, 4029. b) Concepcion, J. J.; Jurss, J. W.; Templeton, J. L.; Meyer, T. J. *Proc. Nat. Acad. Sci., U. S.*   **2008**, 105, 17632.

(28)   McDaniel, N. D.; Coughlin, F. J.; Tinker, L. L; Bernhard, S. *J. Am. Chem. Soc. 2008*, **130**, 210.

(29)   Zong, R.; Thummel, R. P.; *J. Am. Chem. Soc.* **2005**, 127, 12802.

(30)   Geletii, Y. V.; Botar, B.; Kögerler, P.; Hillesheim, D. A.; Musaev, D. G.; Hill, C. L. . *Angew. Chem. Int. Ed.* **2008**, 47, 3896.

(31)   a) Morris, N. D.; Suzuki, M.; Mallouk, T. E. *J. Phys. Chem. A* **2004**, 108, 9115. b) Hoertz, P. G.; Kim, Y.; Youngblood, W. J.; Mallouk, T. E.;   *J. Phys. Chem. B* **2007**, 111, 6845.   c)   Youngblood, W.J.; Lee, S-H.A.; Kobayashi, Y.; Hernandez-Pagan, E.A.; Hoertz, P.G.; Moore, T.A.; Moore, A.L.; Gust, D. and Mallouk, T.E.   *J. Am. Chem. Soc.* **2009**, 131, 926-927.

(32)   a) Kiwi, J.; Graetzel, M. *Angew. Chem., Int. Ed. Engl.* **1978**, 17, 860. b) Kiwi, J.; Graetzel, M. *Angew. Chem., Int. Ed. Engl.* **1979**, 18, 624.

(33)   a) Yagi, M.; Tomita, E.; Sakita, S.; Kuwabara, T.; Nagai, K. *J. Phys. Chem. B* **2005**, 109, 21489. b) Kuwabara, T.; Tomita, E.; Sakita, S.; Hasegawa, D.; Sone, K.; Yagi, M. *J. Phys. Chem. C* **2008**, 112,

3774-3779

(34)   (a) Kanan, M. W.; Nocera, D. G. *Science* **2008**, 321, 1072. (b)Surendranath, Y.; Dincă, M.; Nocera, D. G. *J. Am. Chem. Soc.* **2009**, 131, 2615.

(35)   Fierro, S.; Nagel, T.; Baltruschat, H.; Comninellis, T. *Electrochem. Solid-State Lett.* **2008**, 7, E20-E23.

(36)   Murray, R. W. *Chem. Rev.* **2008**, 108, 2688–2720.

2. Development of functional electrode for electrochemical reduction of oxygen to water toward biofuel cell

2.1. Bilirubin oxidase and $[Fe(CN)_6]^{3-/4-}$ modified electrode allowing diffusion-controlled reduction of oxygen to water at pH 7.0

2.1.1. Introduction

Tsujimura *et al.* have previously shown that bilirubin oxidase (BOD) is a remarkable enzyme exhibiting a high catalytic activity at neutral pH to produce a large bioelectrocatalytic current for the reduction of O_2 to water[1] (Figure 2.1A). This is a significant property of the enzyme allowing the four electron reduction of O_2 at a bio-cathode of a biofuel cell operating at neutral pH[2] and is contrasted to the catalytic property of laccases that are active in acidic pH and accordingly produce appreciable bioelectrocatalytic currents only under acidic conditions[3-5]. BOD is a multi-copper oxidase with a molecular mass of 60 kDa[6,7] catalyzing the oxidation of bilirubin to biliverdin[8] which can use 2,2'-azinobis (3-ethylbenzothiazoline-6-sulfonate) (ABTS) as an electron donor in place of bilirubin[9]. The bioelectrocatalytic behavior of BOD has been studied in detail using ABTS as an electron transfer mediator[1]. The electrocatalytic reduction of O_2 to water occurs at the potential at which ABTS is electrochemically generated from the oxidized form, thus the voltammogram for the O_2 reduction attains a limiting current at 0.40 V vs. Ag/AgCl at pH 7.0 with the half-wave potential, 0.49 V, close to the redox potential of ABTS,
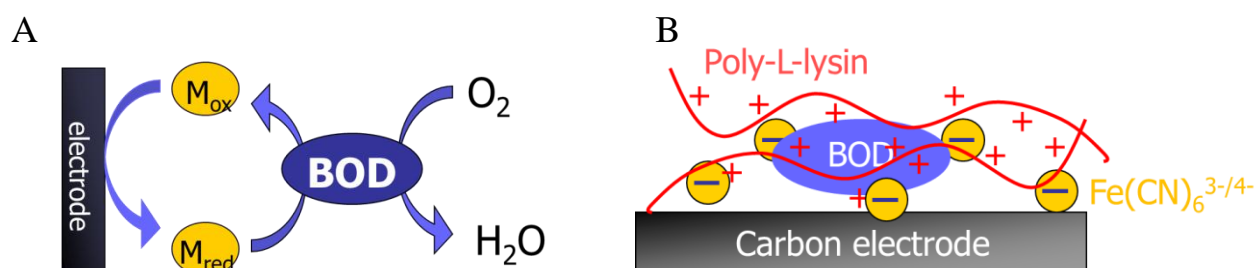
Figure 2.1. (A) Electrochemical oxygen reduction by using BOD as catalyst (B) Immobilization of BOD and $Fe(CN)_6^{3-/4-}$ with poly-L-lysine on glassy carbon electrode

0.505 V, which is 0.11 V more negative than the redox potential of dioxygen/water, $E'O_2/H_2O = 0.615$ V, at this pH. Kinetic analysis of the bioelectrocatalytic current has revealed that the BOD reaction has a high catalytic constant, $k_{cat} = 2.3 \times 10^2$ s^{-1}, with the Michaelis constant $K_{ABTS} = 11$ μM for ABTS. The large

catalytic constant and the small Michaelis constant are ideal properties for the enzyme to be used in a bio-cathode reaction of a biofuel cell. However, there is a problem that it is difficult to immobilize ABTS on an electrode surface for obtaining a higher current density. Heller *et al*. have used BOD to realize the bioelectrocatalytic reduction of O_2 at pH 7.4 and at 37.5 $^\circ$C using a redox polymer as a mediator, in which BOD has been cross-linked with the polymer on carbon felt[10].

2.1.2. Electrochemistry of BOD-$[Fe(CN)_6]^{3-/4-}$ -PLL glassy carbon electrode

Here the author on the use of $[Fe(CN)_6]^{3-/4-}$ as a mediator, which is easily immobilized on an electrode surface by an electrostatic entrapment with a cationic polymer[11]. Both BOD and $[Fe(CN)_6]^{3-}$ were entrapped with a cationic polymer poly-L-lysine (PLL) on a glassy carbon electrode (Figure 2.1B). Stock solution (0.2 ml) was prepared by dissolving 6 mg of BOD (EC 1.3.3.5, from *Myrothecium verrucaria*, a gift from Amano Pharmaceutical Co. Japan) and 4.4 mg of PLL (molecular weight 8000, purchased from Peptide Institute INC. Osaka) in a phosphate buffer (0.0465 M, pH 7). 10 µL of the solution was syringed on the surface of a glassy carbon electrode (GCE) (φ = 3 mm). After allowing evaporation of the solvent, the electrode was immersed in 5 mM potassium hexacyano ferrate (III) for 5 min. Then the electrode was rinsed with a distilled water and 5 µL of 2.2 % PLL solution was further syringed to cover the BOD-$[Fe(CN)_6]^{3-}$-PLL layer. As shown in Figure 2.2, the BOD-$[Fe(CN)_6]^{3-/4-}$ -PLL GCE produced peak-shaped cyclic voltammograms (CVs) in a deaerated solution. The peak current increases linearly with the increase in the scan rate, which is typical of the current due to a surface-confined redox species, and the waves are attributable to the redox reaction of $[Fe(CN)_6]^{3-/4-}$ electrostatically entrapped in the BOD-$[Fe(CN)_6]^{3-}$-PLL layer on the GCE surface. The peak potentials of the anodic and cathodic waves shift positive and negative directions, respectively, with increasing scan rate, which reflects an irreversible nature of the electrode reaction of $[Fe(CN)_6]^{3-/4-}$.The amount of the $[Fe(CN)_6]^{3-/4-}$ confined on the GCE is calculated as 0.85 nmol from the areas of the peak-shaped waves, which leads 1.2×10^{-8} mol/cm^2 with φ = 3 mm of the GCE. It is noted in the CVs that the mid-potential (formal potential) of $[Fe(CN)_6]^{3-/4-}$, 240 mV vs Ag/AgCl, is

35 mV more positive than the formal potential of $[Fe(CN)_6]^{3-/4-}$ in solution. This is attributed to the electrostatic interaction between $[Fe(CN)_6]^{3-/4-}$ and PLL; simple calculation reveals that the shift of 35 mV corresponds to 52 times stabilization of $[Fe(CN)_6]^{4-}$ compared with $[Fe(CN)_6]^{3-}$. The positive shift is a favorable direction allowing the occurrence of a bioelectrocatalytic current at a less negative potential.

When the same solution as in Figure 2.2 is air-saturated, the BOD-$[Fe(CN)_6]^{3-/4-}$-PLL GCE produces large cathodic currents as illustrated in Figure 2.3. The cathodic current has an irreversible character, and the peak current increases linearly with the square root of the scan rate. This is typical of an irreversible voltammogram of a redox spesies in solution. Thus I attribute the voltammogram to the reduction of O_2.

Applying the theory of a totally irreversible voltammogram[12]:

$$i_p = n(2.99 \times 10^5)\alpha^{\frac{1}{2}} A c_j^* D^{\frac{1}{2}} v^{\frac{1}{2}} \qquad (2.1)$$

(where i_p, n, α, A, c^*, D, and v are the peak current, number of electrons, transfer coefficient, electrode surface area, bulk concentration of the species j, diffusion coefficient of j and the scan rate, respectively,). The author obtain the D value of 5.2×10^{-5} cm^2 s^{-1} from the dependence of i_p on $v^{1/2}$ with $n = 4$ (for O_2 reduction to water), $A = 0.071$ cm^2 (the area of the GCE with $\varphi = 3$ mm), $c_j = 0.25$ mM (the concentration of O_2) and $\alpha = 0.38$. The α value was estimated from the CVs by the equation:[12]

$$\left| E_p - E_{1/2} \right| = 47.7/\alpha \ \text{mV} \qquad (2.2)$$

(where E_p and $E_{p/2}$ are the peak potential and the potential where the current is at half the peak value). Almost the same D value, 4.4×10^{-5} cm^{2}s^{-1}, was obtained from the chronoamperometry at the BOD-$[Fe(CN)_6]^{3-/4-}$-PLL GCE at –0.1 V. The value of $5.2 – 5.0 \times 10^{-5}$ cm^2 s^{-1} is somewhat larger than the reported D value of O_2, $2.0 – 2.5 \times 10^{-5}$ cm^2 s^{-1}.[13] This may be attributed to the fact that the BOD-$[Fe(CN)_6]^{3-/4-}$-PLL layer covering the GCE should be larger than the area of the bare GCE and is and is understandable as the roughness factor of 1.6 of the electrode.
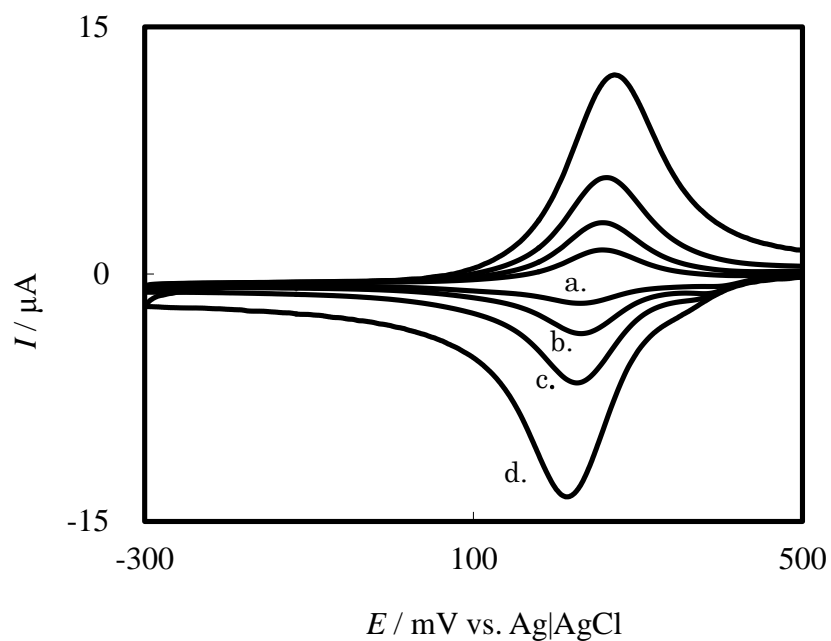
Figure 2.2. Cyclic voltammograms of a BOD-Fe(CN)$_6^{3-/4-}$-PLL GCE in a deaerated phosphate buffer of pH 7.0 at the scan rates: a, 5; b, 10; c, 20; d, 50 mV/s
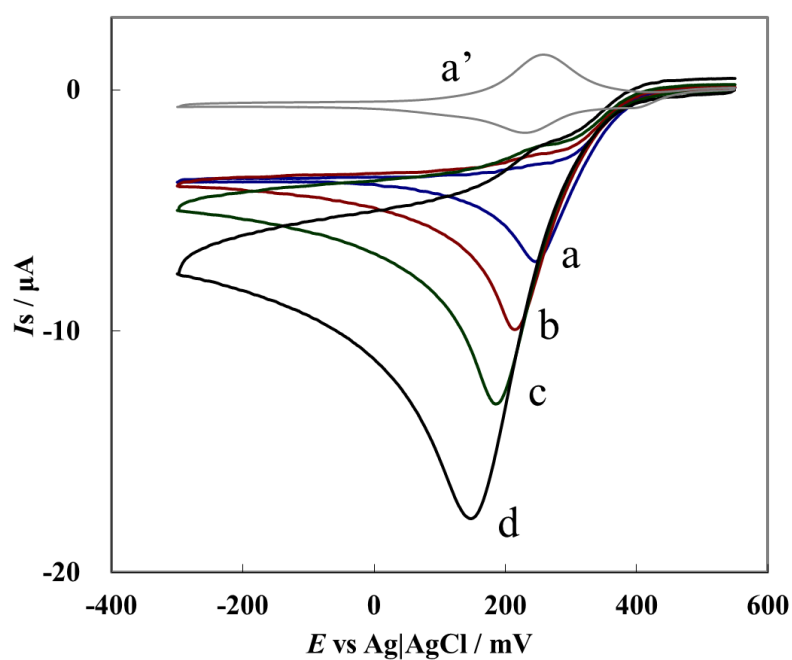
Figure 2.3. CVs of a BOD-[Fe(CN)$_6$]$^{3-/4-}$-PLL GCE in an air-saturated phosphate buffer of pH 7.0 at the scan rates: a, 5; b, 10; c, 20; d, 50 mV/s. a': CV in a deaerated solution at the scan rate 5 mV/s.
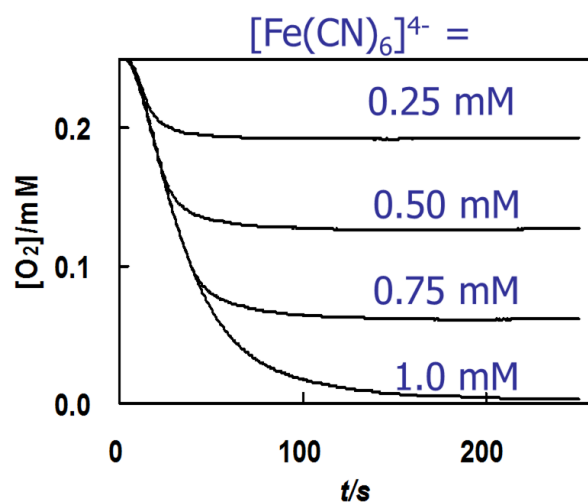
Figure 2.4. Measurements of the stoichiometry of the BOD reaction confirming that the reduction of one mol of O_2 consumed four mols of $[Fe(CN)_6]^{4-}$ by using Clark's oxygen electrode
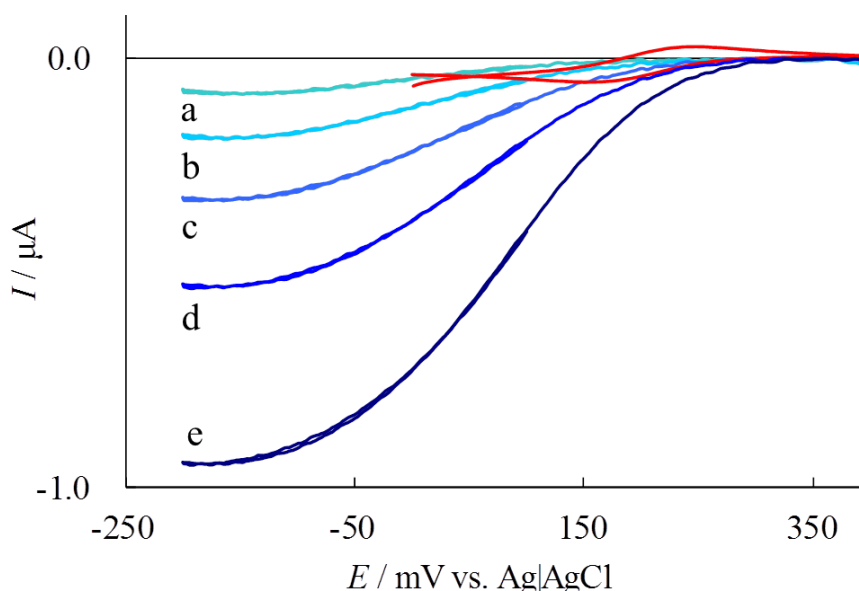
Figure 2.5. CVs of oxygen reduction with BOD and $[Fe(CN)_6]^{4-}$ in an oxygen-saturated phosphate buffer of pH 7.0 at the scan rate 5 mV/s. $[Fe(CN)_6]^{4-}$ is a) 1, b) 2.5, c) 5, d) 10 and e) 25 μM. Red line shows the CV of only 10 μM $[Fe(CN)_6]^{4-}$ without BOD. Electrode is bare glassy carbon electrode ($\varphi = 3$ mm).

Thus, I may say that Figure 2.3 is, as far as I aware, the first demonstration of the diffusion-controlled CVs for the four-electron reduction of O_2 to water at neutral pH. It should be noted, however, that the electrochemical reduction of O_2 proceeds indirectly by the BOD-catalyzed reduction through the mediation of $[Fe(CN)_6]^{3-/4-}$ in the BOD-$[Fe(CN)_6]^{3-/4-}$-PLL layer. The α value is thus attributed to the electrode reaction of $[Fe(CN)_6]^{4-}$, though the overall reaction is the reduction of O_2. The validity of eq. 2.1 and eq. 2.2 for the

23

analysis of the CVs in Figure 2.3 is not self-evident, but the use of the equations seems to be appropriate. This idea is supported by the fact that the D values determined from the CVs and the chronoamperogram agree well as mentioned above. Measurements of the stoichiometry of the BOD reaction confirmed that the reduction of one mol of O_2 consumed four mols of $[Fe(CN)_6]^{4-}$ (Figure 2.4). Figure 2.5 and Figure 2.6 shows the CVs of dependence of concentration of $[Fe(CN)_6]^{4-}$ against BOD and plots of the concentration dependence of mediator and BOD in phosphate buffer solution. The catalytic constant (k_{cat}) and the Michaelis constants (K_{Med}) can calculated from Matsumoto equation[12]:

$$\frac{I_s^{lim}}{n_M FA\sqrt{(n_S/n_M)D_M k_{cat} K_M [E]}} = \sqrt{2\left[\frac{[M]^*}{K_M} - \ln\left(1+\frac{[M]^*}{K_M}\right)\right]} \qquad (2.3)$$

Measurements of the enzyme kinetics of the BOD reaction revealed that the catalytic constant (k_{cat}) is 200 s^{-1} and the Michaelis constants for O_2 and $[Fe(CN)_6]^{4-}$ are 50 μM and 2.7 μM, respectively. The large catalytic constant is indispensable for realizing the mass transfer-controlled bioelectrocatalytic current. The small Michaelis constants are also favorable for the mass transfer-controlled overall reaction. This is because that the BOD reaction remains constant independent of the concentrations of both O_2 and $[Fe(CN)_6]^{4-}$ down to those close to the values of the Michaelis constants, keeping the fast BOD reaction even in the small O_2 concentrations at the surface of the BOD-$[Fe(CN)_6]^{3-/4-}$-PLL layer on the GCE.

I have observed a steady-state limiting current as large as 150 μA (2.1 mA/cm^2 by the calculation using $A = 0.071$ cm^2) at the BOD-$[Fe(CN)_6]^{3-/4-}$-PLL GCE in a dioxygen-saturated phosphate buffer (pH 7.0) when the solution was stirred with a stirring bar (Figure 2.7). The O_2 reduction at more positive potentials would be expected with the use of other kinds of cyano-metal complexes. For example, $[W(CN)_8]^{3-/4-}$ is also good mediator for BOD and can be modified by same poly ion complex using PLL although its potential is 0.32 V vs. Ag|AgCl which is more positive potential than one of $[Fe(CN)_6]^{3-/4-}$.[13]
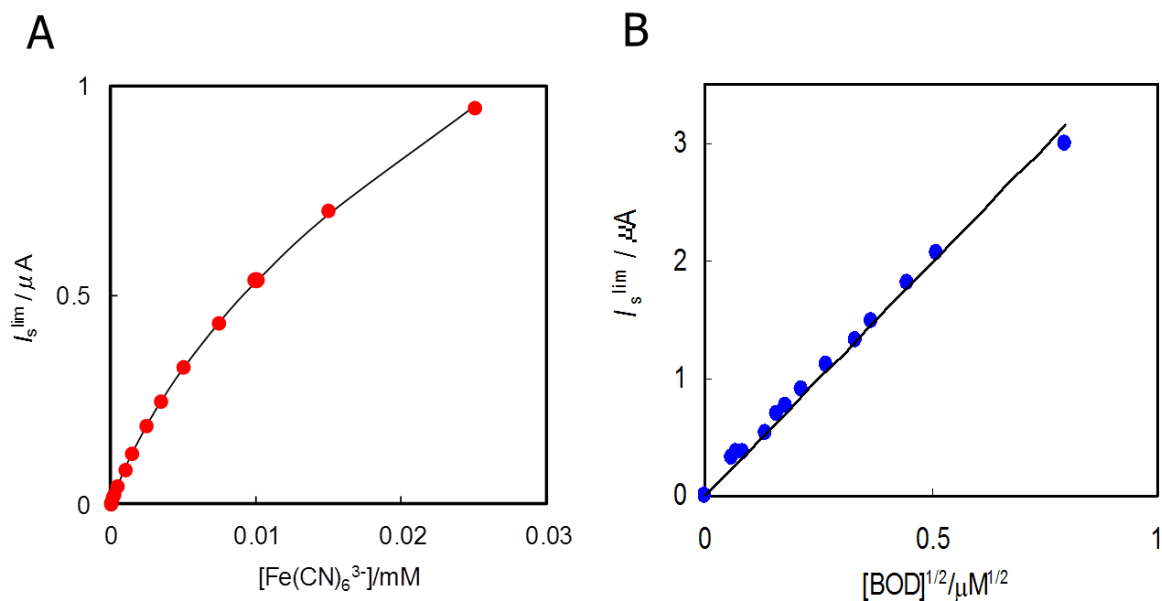
Figure 2.6. A) Dependence of catalytic limiting current dependent on concentration of $[Fe(CN)_6]^{4-}$ at 50 mM phosphate buffer at pH 7.0 including 37.7 nM of BOD.

B) Dependence of catalytic limiting current dependent on concentration of BOD at 50 mM phosphate buffer at pH 7.0 including 100 μM of $[Fe(CN)_6]^{4-}$. Both electrode is bare glassy carbon electrode ($\varphi = 3$ mm).

2.1.3. Electrochemistry of porous carbon electrode modified BOD-$[Fe(CN)_6]^{3-/4-}$

A higher current density per projected surface area will be expected with the use of carbon materials of a large surface to volume. Carbon felt electrode (CF, BO050 from Toray) is a sheet of carbon fiber which has a high surface electrode and flexibility. BOD-$[Fe(CN)_6]^{3-/4-}$-PLL CF electrode can be easily to prepare because BOD, cyano-metal complexs and PLL can easily elute into the CF electrode although other carbon material like carbon paper and carbon powder electrode surface is water-shedding surface rather than hydrophilic[1]. CF electrodes (3 mm diameter = 0.0707 cm^2), on which BOD and $[W(CN)_8]^{3-/4-}$ were immobilized with PLL, were fixed on a glassy carbon electrode (3 mm diameter) with nylon net. The performance of this CF fixed electrode can be measured by rotating disk electrode system (RDE) (Figure 2.8A).

25
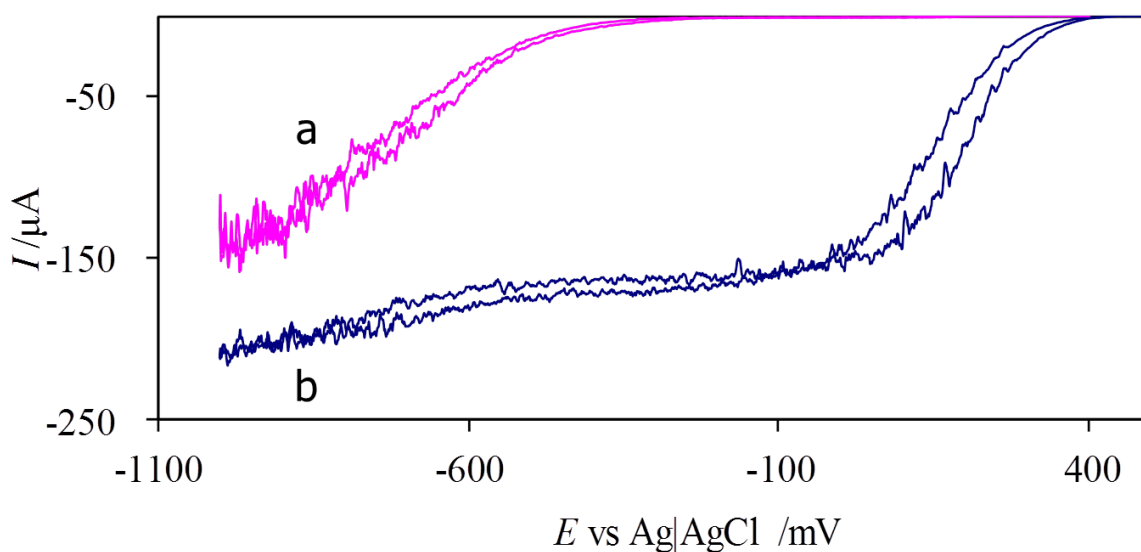
Figure 2.7. CVs of (a) bare GCE and (b) BOD-[Fe(CN)$_6$]$^{3-/4-}$-PLL GCE in an oxygen-saturated phosphate buffer of pH 7.0 at 20 mV/s when the solution was stirred with a stirring bar.

Moreover, plasma treatment can improve CF electrode to more hydrophobic surface and increase surface area[14]. After treated by microwave for 30 second at 600 W, BOD-[W(CN)$_6$]$^{3-/4-}$-PLL modified CF electrode performance is obviously improved shown as Figure 2.8A using rotating disk electrode. At 300 rpm, current peak is appeared because of exhaustion of oxygen. The catalytic limiting current density is no deference between with treatment and without treatment because oxygen mass transfer is restricted by rotating speed. However, the catalytic current density of functional electrode with treatment was about 1.8 times higher than one of electrode without treatment because the catalytic current density is determined by capability of functional electrode. The limiting current density of BOD-[W(CN)$_8$]$^{3-/4-}$-PLL CF fixed disk electrode after microwave treatment reached about 20 mA/cm^2 at 3000 rpm ($\omega^{1/2}$ = 17.7 s^{-1}). This catalytic limiting current density is approximately 10 times higher than plane glassy carbon electrode modified BOD and [Fe(CN)$_6$]$^{3-/4-}$ at a stirring condition because of increasing the electrode surface area by pours structure of carbon felt electrode.   The catalytic current density is increased to 50 mA/cm^2 with the sheets number of BOD-[W(CN)$_8$]$^{3-/4-}$-PLL CF on disk electrode in case of more than 3000 rpm. This indicated that electrical resistance of BOD-[W(CN)$_8$]$^{3-/4-}$-PLL CF electrode is tolerable small level and electron transfer between CF

electrode and electron mediator is fast after treatment. However, Levich plots of this BOD-$[W(CN)_8]^{3-/4-}$-PLL

CF electrode is not linear like Figure 2.8B. The catalytic current was increasing slowly when the rotating

speed is below 600 rpm ($\omega^{1/2}$ = 7.9 s^{-1}). On the other hand, the slope is increase above 600 rpm. It is likely

that mass transfer is easily accessible into CF porous structure above 600 rpm because flow by rotating speed

is enough. Nevertheless, enough forced flow is strongly needed to demonstrate the capability of pours

electrode modified BOD and mediator in order to supply oxygen and proton inside of its structure.
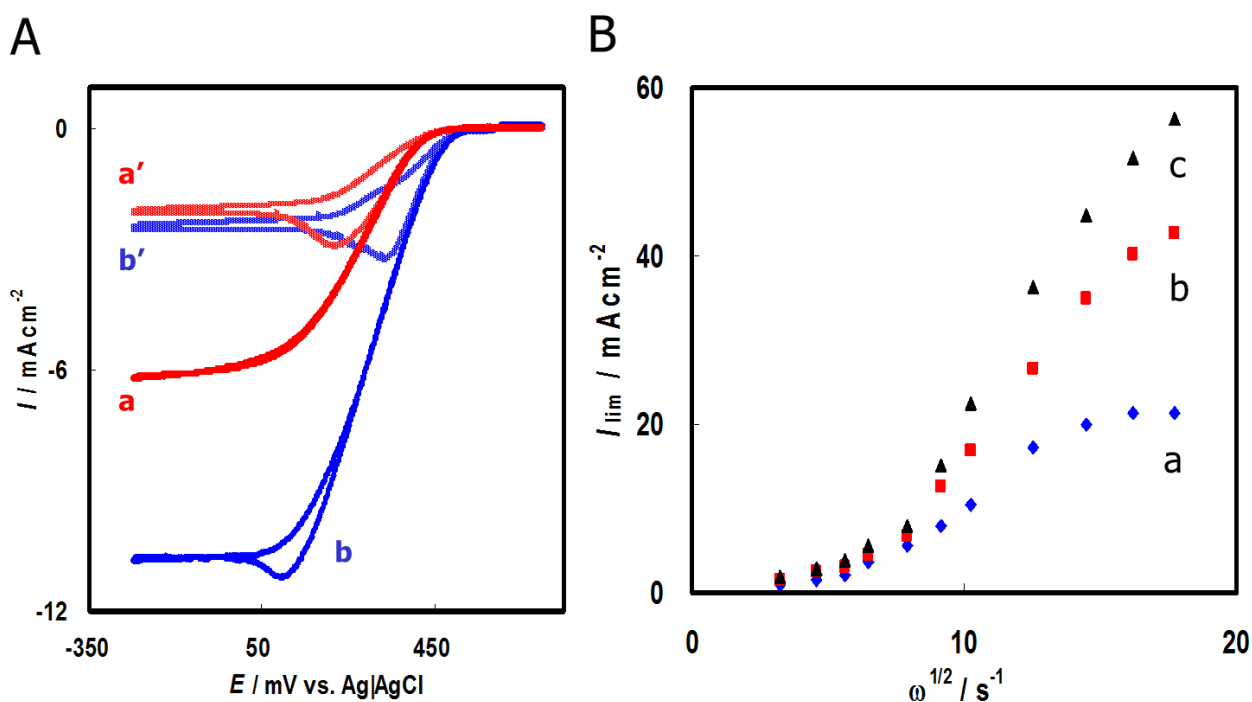
Figure 2.8. A) CVs of BOD-$[W(CN)_8]^{3-/4-}$-PLL CF fixed disk electrode in an oxygen-saturated phosphate
buffer of pH 7.0 at 20 mV/s (a') at 300 rpm and (a) 1000 rpm. CVs of BOD-$[W(CN)_8]^{3-/4-}$-PLL CF fixed disk
electrode after microwave treatment in an oxygen-saturated phosphate buffer of pH 7.0 at 20 mV/s (b') at
300 rpm and (b) 1000 rpm.
  B) Levich plots of the catalytic limiting current of BOD-$[W(CN)_8]^{3-/4-}$-PLL CF fixed disk electrode after
microwave treatment in an oxygen-saturated phosphate buffer of pH 7.0 at 20 mV/s. The number of
BOD-$[W(CN)_8]^{3-/4-}$-PLL modified CF sheet is (a) one, (b) two and (c) three.

2.1.4. Conclusions

In conclusions, the author reported that a novel functional electrode which is CF electrode immobilized BOD and cyano-metal complex with PLL, which oxygen reduction current density is about 20-30 mA/cm^2 at 2000 rpm at oxygen saturated conditions. However how oxygen and proton supply into BOD-cyano-metal complex -PLL CF electrode continually is important to achieve high catalytic current.

2.1.5. Experimental

Stock solution (0.2 ml) was prepared by dissolving 6 mg of BOD (EC 1.3.3.5, from *Myrothecium verrucaria*, a gift from Amano Pharmaceutical Co. Japan) and 4.4 mg of poly-L-lysine (molecular weight 8000, purchased from Peptide Institute INC. Osaka) in a phosphate buffer (0.0465 M, pH 7). 10 μL of the solution was syringed on the surface of a glassy carbon electrode (GCE) (φ = 3 mm). After allowing evaporation of the solvent, the electrode was immersed in 5 mM potassium hexacyano ferrate (III) for 5 min. Then the electrode was rinsed with a distilled water and 5 μL of 2.2 % PLL solution was further syringed to cover the BOD-[Fe(CN)$_6$]$^{3-}$-PLL layer. Electrochemical measurements were performed using a BAS electrochemical analyzer in a three-electrode system in which GCE was used as a working electrode. Rotating-disk electrode experiments were carried out with RDE-2 rotating disk electrode system (BAS). Carbon felt (CF) electrodes (3 mm diameter = 0.071 cm^2), on which BOD and ferricyanide were immobilized with PLL, were fixed on a glassy carbon electrode (3 mm diameter) with nylon net. A Pt wire and Ag|AgCl|sat. KCl electrode were used as a counter electrode and reference electrode, respectively. All potentials are referred to the Ag|AgCl|sat. KCl electrode.

References and Notes

(1)   Tsujimura, S.; Tatsumi, H.; Ogawa, J.; Shimizu, S.; Kano, K.; Ikeda, T. *J. Electroanal. Chem.* **2001**, 496, 69.

(2)   Tsujimura, S.; Fujita, M.; Tatsumi, H.; Kano, K.; Ikeda, T. *Phys. Chem. Chem. Phys.* **2001**, 3, 1331.

(3)   Tarasevich, M. R.; Yaropolov, A.I.; Bogdanovskaya, V.A.; Varfolomeev, S.D. *Bioelectrochem. Bioenerg.* **1979**, 6, 393.

(4)   Palmore, G. T. R.; Kim, H.-H. *J. Electroanal. Chem.* **1999**, 464, 110.

(5)   Barton, S. C.; Kim, H.-H.; Binyamin, G.; Zhang, Y.; Heller, A. *J. Phys. Chem. B,* **2001**, 105, 11917; Barton, S. C.; Kim, H.-H.; Binyamin, G.; Zhang, Y.; Heller, A. *J. Am. Chem. Soc.* **2001**, 123, 5802.

(6)   Tanaka, N.; Murao, S. *Agric. Biol. Chem.* **1982**, 46 2499.

(7)   Gotoh, Y.; Kondo, Y.; Kaji, H.; Takeda, A.; Samejima, T. *J. Biochem.* **1989**, 106 621.; Shimizu, Kwon, J-H.; Sasaki, T.; Satoh, T.; Sakurai, N.; Sakurai, T.; Yamaguchi, S.; Samejima, T. *Biochemistry* **1999**, 38, 3034.; Shimizu, Sasaki, T.; Kwon, J-H.; Odaka, A.; Satoh, T.; Sakurai, N.; Sakurai, T.; Yamaguchi, S.; Samejima, T.; *J. Biochem.* **1999**, 125 662.

(8)   Murao, S.; Tanaka, N. *Agric. Biol. Chem.* **1982,** 46 2031.

(9)   Xu, F.; Shin, W.; Brown, S.H.; Wahleithner, J.A.; Sundaram, U.M.; Solomon, E. I. *Biochim. Biophys. Acta* **1996**, 1292 303.

(10)   Mano, N.; Kim, H.-H.; Zhang, Y.; Heller, A. *J. Am. Chem. Soc.* **2002**, 124, 6480.; Mano, N.; Kim, H.-H.; Heller, A. *J. Phys. Chem. B.* **2002**, 106, 8842.

(11)   Ikeda, T.; Shiraishi, T.; Senda, M. *Agric. Biol. Chem.* **1988**, 52, 3187.

(12)   Matsumoto, R.; Kano, K.; Ikeda, T. *J. Electroanal. Chem.* **2002**, 535, 37–40

(13)   Tsujimura, S.; Kawaharada, M.; Nakagawa, T.; Kano, K.; Ikeda, T. *Electrochem.Commun.* **2003**, 5,138–141

(14)   Horita, K.; Nishibori, Y.; Takao, O. *Carbon* **1996**, 34 (2), 217–222

2.2. Water-repellent-treated enzymatic electrode for passive air-breathing biocathodic reduction of oxygen

2.2.1. Introduction

Biofuel cells are highly promising next-generation energy conversion devices, which permit the use of safe and high–energy-density fuels such as glucose under ambient conditions[1-5]. Multi-copper oxidases, including laccase and bilirubin oxidase (BOD), have been developed as oxygen-reducing cathodes for bioelectrocatalytic applications; among the family of multi-copper oxidases, BOD is currently the most promising electrocatalyst for this purpose, operating under neutral pH conditions and room temperature[6-17]. Significant research efforts toward the development of biocathode systems using highly active enzymes, redox mediators, and porous electrode materials have established that catalytic current density is dependent on the oxygen supply, because oxygen has low solubility in water[13, 18]. Although biocathode performance can be improved by solution stirring and/or bubbling oxygen gas into the system[18], such active-type biofuel cell systems are not suited for practical use as they typically require external power, which makes the system operation complicated. In order to increase the oxygen supply and current density, a greater degree of control over hydrophobicity (for oxygen transport) and hydrophilicity (for enzyme reactivity and ion transport) is crucial. Kano *et al.* reported an air-breathing biocathode that used polytetrafluoroethylene (PTFE) both as a binder for holding carbon materials and as a water repellent[19, 20]. A carbon slurry prepared by mixing Ketjen Black and PTFE in 2-propanol was applied on the current collector (Toray carbon paper), followed by application of the enzyme solution on the resulting water-repellent carbon electrode. The steady-state current density catalyzed by CueO from *Escherichia coli*, a type of multi-copper oxidase, reached as high as 20 mA cm^{-2} at 0 V in 1.0 M citrate buffer solution at pH 5.0 in a passive cell system. Nishizawa *et al.* reported that Ketjen Black or carbon nanotube coating on BOD-modified face on the electrode enhanced the performance further to 2.0 mA cm^{-2} because the hydrophobic nature of that coating controls excess penetration of solution into the CF electrodes[21]. Atanassov *et al.* reported carbon paper with a pressed layer of teflonized carbon

black as gas diffusion layer[22]. In order to achieve higher current density, it is important to make tri-phase which is interphase between electrolyte in porous electrode, catalysis and air, especially inside of porous electrode. Nevertheless, it was difficult to increase the hydrophilic enzyme and mediator loadings for such hydrophobic porous carbon electrodes while keeping its water-repellent surface after immobilizing these components.

2.2.2. Enzyme and mediator modified CF electrode with water-repellent

To improve cathodic performance by supplying oxygen gas from air, the author initially applied a semipermeable membrane as a separator between an anode and a cathode; the prepared biocathode was then exposed to air. Such a membrane allows for proton transfer from the anode to the cathode, but prevents the cathode from flooding[5]. Furthermore, the author improved the cathodic current density by employing imidazole buffer instead of the more commonly used phosphate buffer in order to prevent pH changes in the electrode surface vicinity during the continuous supply of oxygen and protons to the electrode surface.
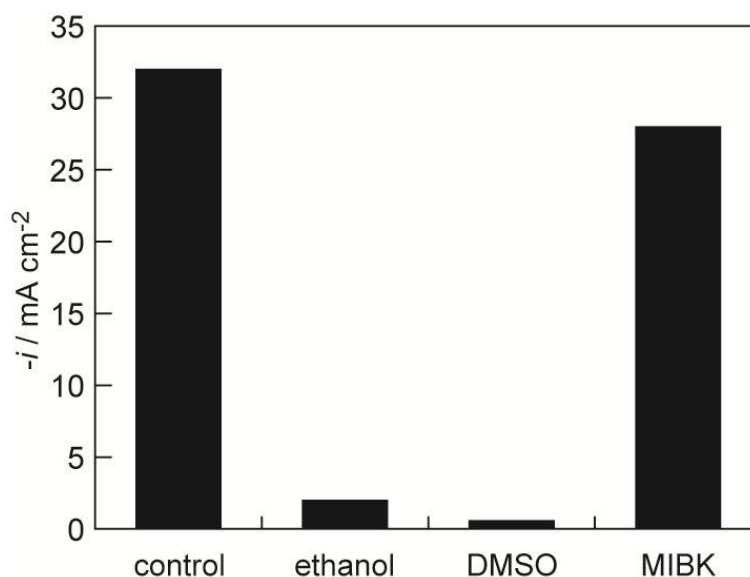
Figure 2.9. Effect of organic solvent on the biocathode modified with BOD and ferricyanide with PLL. Relative current densities at 0 V of the biocathodes against untreated electrode at 1000 rpm in 50 mM sodium phosphate buffer (pH 7.0) saturated with O_2. The electrodes were rotated at 2000 rpm.

31

In efforts to improve the trade-off relation between oxygen and proton supply, the present study reports investigations on the modification of a porous carbon electrode immobilized with BOD and ferricyanide/poly-L-lysine (PLL) by application of a water repellent dissolved in methyl isobutyl ketone. This method allows for greater control of the enzyme-modified electrode hydrophobicity without damaging the enzyme; a catalytic current density of 25 mA cm^{-2} at pH 7 could be achieved under passive conditions.

For convenient application, the water repellent agents must be dissolved in organic solvents; therefore, the author first investigated the effect of organic solvent on enzymatic stability/activity by exposing the enzyme-modified electrode to a number of organic solvents. The CF disc electrode without organic solvent treatment rotated at 2000 rpm showed an oxygen reduction current of 32 mA cm^{-2} at 0 V in 50 mM phosphate buffer solution saturated with O_2 at pH 7. The enzyme- and mediator-modified electrode was then exposed to organic solutions (40 μL of EtOH, DMSO, or MIBK). Figure 2.9 shows the influence of organic solvent on the biocathodic oxygen reduction current. Although EtOH and DMSO solutions significantly deteriorated the electrode activity, MIBK, having a lower dielectric constant and solubility in water than EtOH and DMSO, did not affect the enzyme electrode activity. It is likely that the hydrophilic enzyme and mediator are not evenly distributed in MIBK solution; thus, enzyme structure, e.g. hydrogen bonding, hydrophobic packing, etc., was hardly influenced by the solvent. BOD dissolved in buffer solution was also stable for a few hours after mixing with MIBK solution (data not shown). The author chose MIBK as a solvent for water repellents, as they are readily soluble in MIBK solution, and MIBK can be evaporated immediately.

Figure 2.10A shows the biocathode liner sweep voltammograms with and without water-repellent treatment in imidazole buffer solution (2.0 M, pH 7.0). The experimental setup is illustrated in Figure 2.10B. Under an Ar atmosphere, a ferricyanide reduction current was observed in the cell, but a catalytic current for oxygen reduction was observed (Figure 2.10A, curve 1). In air, the biocathode showed a steady-state catalytic current of 8 mA cm^{-2} at 0 V. The oxygen gas penetrating the PTFE membrane was supplied to the enzyme layer. The catalytic current was observed to increase on water-repellent treatment and the magnitude of the catalytic current depended on the amount of the water-repellent. Curves 3, 4, and 5 (Figure 2.10A)
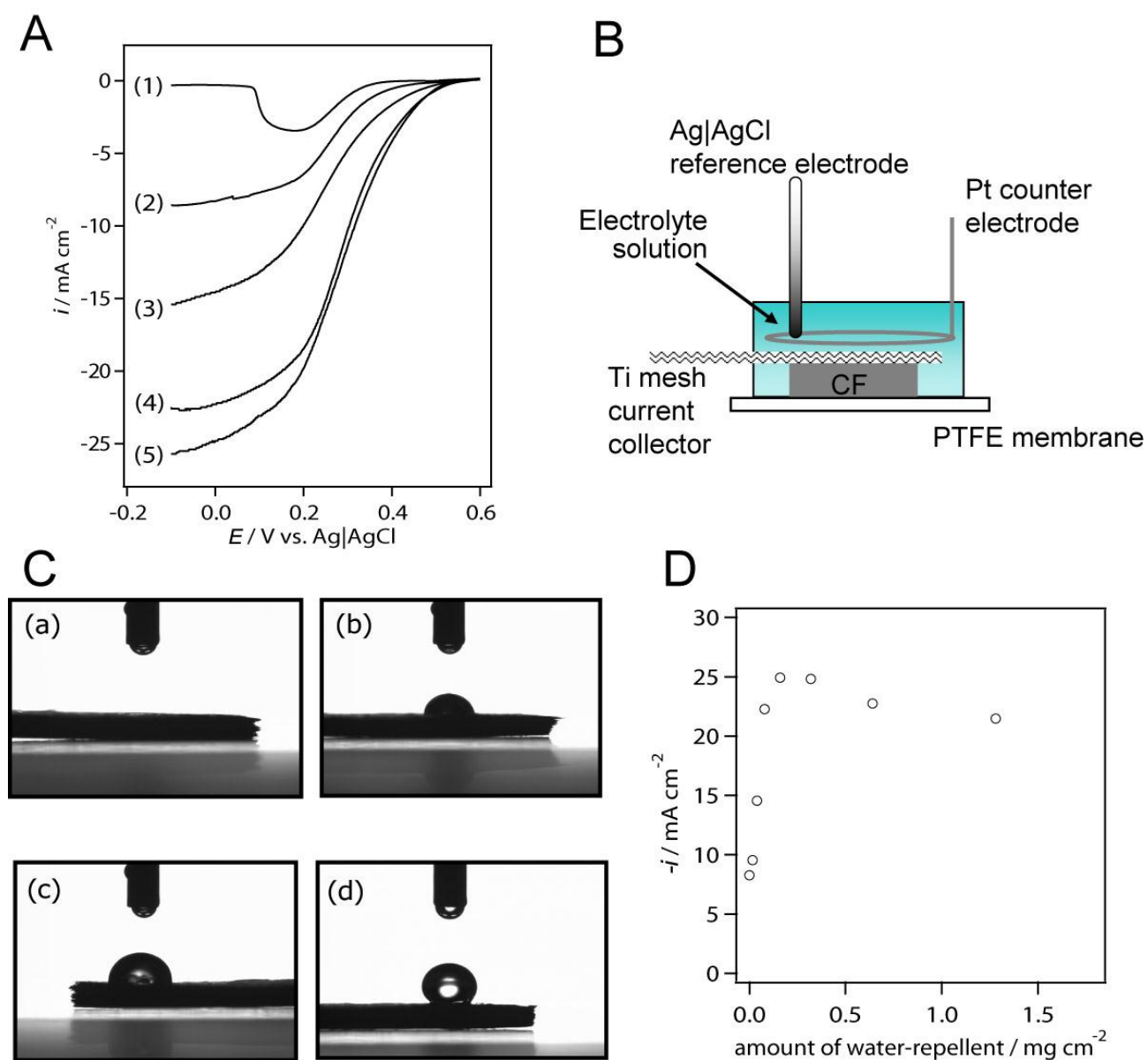
Figure 2.10. A) Liner sweep voltammograms of biocathodes without water repellent treatment (2), and coated with 0.08 mg (3), 0.16 mg (4), and 0.32 mg (5) of water repellents under air. Curve (1) was observed under Ar. Conditions: 2.0 M imidazole/HCl buffer (pH 7.0); scan rate, 1 mV s^{-1}.

B) Schematic illustration of the experimental cell setup.

C) Biocathode contact angles without (a) and with water repellent treatment (b–d). The biocathodes were coated with 0.08 mg (b), 0.16 mg (c) and 0.32 mg (d) water repellents.

D) Dependence of catalytic current densities on water-repellent amounts.

were obtained using a biocathode treated with 0.08, 0.16, and 0.32 mg water repellent material, respectively. The biocathode treated with 0.32 mg water repellent showed a current density of 25 mA cm^{-2} at 0 V under air conditions. Contact angles between the CF electrode surface and buffer droplet became larger with increased water repellent coverage (Figure 2.10C) and both side of electrode and inside of electrode also have water repellency (data not shown). The increase in catalytic current depending on the hydrophobicity was attributed to the oxygen transport in the biocathode porous structure. However, a current decrease was observed on the electrode coated with more than 0.32 mg of water repellent because of the insufficient proton transfer through the permeated electrolyte within the CF electrode (Figure 2.10D). Figure 2.11A shows the constant potential electrolysis of O_2 using the electrolysis cell described above, in which the CF biocathode was coated with 0.32 mg of the water repellent, and the previously reported cell using a semipermeable membrane. The buffer used was 2.0 M imidazole at pH 7.0. The steady-state current was 20 mA cm^{-2} at 0.25 V, a twofold increase over that using the previous biocathode system[23]. Figure 2.11B shows investigations on the dependence of buffer concentration and O_2 supply on the catalytic current. In our previous biocathode system, the catalytic current was slightly dependent on both buffer and O_2 concentrations, suggesting that the ion (proton)-transfer step through the semipermeable membrane might limit the catalytic current. On the other hand, the performance of the new sink-type biocathode strongly depended on the buffer concentration up to ca. 2.0 M. The catalytic current reached 32 mA cm^{-2} using the biocathode under O_2-saturated conditions, very similar to the catalytic limiting current when enough oxygen and protons are supplied by rotating the electrode at 2000 rpm (Figure 2.9).

2.2.3. Conclusions

In conclusions, the author report a water repellent–modified biocathode with immobilized BOD and ferricyanide with PLL that retains its enzymatic activity after treatment with a solvent/repellent solution. MIBK was effective in depositing the fluorinated/silicon-based water repellent polymer. The oxygen reduction catalytic current was 24 mA cm^{-2} at 0 V, and 32 mA cm^{-2} at 0 V, under air-saturated and

oxygen-saturated conditions, respectively.
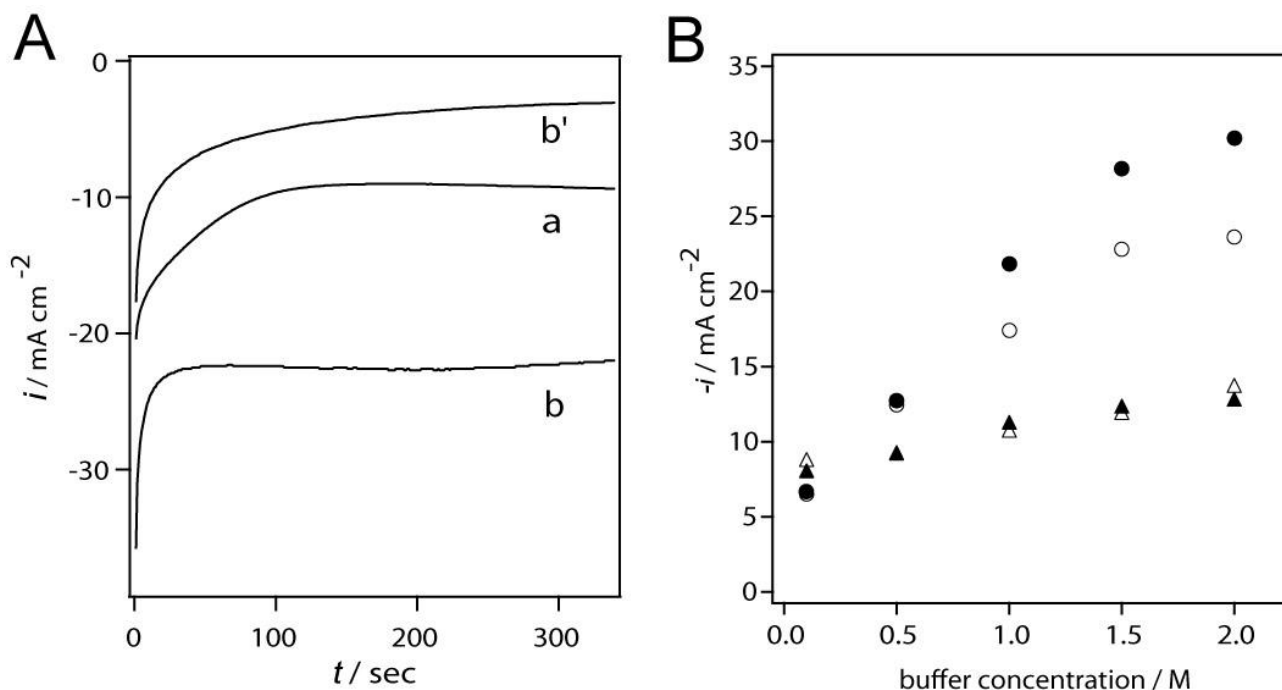
Figure 2.11. A) Time-dependence of oxygen reduction currents poised at 0.25 V. Biocathode using semipermeable membrane system[5] (a), sink-type biocathode system in air using water repellent biocathode (b) and biocathode without water repellent treatment (b').

B) Dependence of catalytic current after 5 minute at 0 V on the biocathode buffer concentration using a semipermeable membrane (triangle) and water repellent biocathode (circle). Open and closed symbols represent air and O_2 conditions, respectively.

2.2.4. Experimental

BOD from *Myrothecium sp*. were purchased from Amano Enzyme (Nagoya, Japan). Poly-L-lysine (PLL, MW approximately 8,000) was purchased from Peptide Institute Inc., Ltd. (Osaka, Japan). The biocathode was prepared by successive application of a BOD solution (20 μL, 100 mg/mL), PLL solution (20 μL, 2 wt%) and ferricyanide (20 μL, 200 mM) on a carbon felt (CF, BO050 from Toray) electrode (1 cm^2) after treated by microwave for 30 second at 600 W[5]. Water repellents were prepared as follows: Scotchgard^{TM} for fabric and cloth protector (Sumitomo 3M Ltd. Tokyo, Japan), a water-repelling fluorinated silicone-type polymer, was sprayed into a beaker and completely dried for 24 h under anhydrous conditions.

Original solvent is acetone, isopropanol and ethanol[24]. After determination of total water repellent weight, it was dissolved in methyl isobutyl ketone (MIBK). Water-repellent treatment of the biocathode (1 cm^2) modified with BOD and ferricyanide with PLL was carried out by adding the water repellent in MIBK (40 μL) and drying for 3 h in a desiccator. An electrochemical cell was assembled for biocathode tests using an acrylic chassis with a titanium mesh as the current collector and PTFE sheet (EN0701405 from Nippon Donaldson, Tokyo, Japan) as a gas-permeable membrane. Electrochemical measurements were performed using a 1480 Multi-Stat (Solartron Analytical) in a three-electrode system in which the biocathode was used as a working electrode. Rotating-disk electrode experiments were carried out with an ALS electrochemical analyzer model 760E (CH instruments) and RDE-2 rotating disk electrode system (BAS). Carbon felt (CF) electrodes (6 mm diameter = 0.28 cm^2), on which BOD and ferricyanide were immobilized with PLL, were fixed on a glassy carbon electrode (3 mm diameter) with nylon net[16]. A Pt wire and Ag|AgCl|sat. KCl electrode were used as a counter electrode and reference electrode, respectively. All potentials are referred to the Ag|AgCl|sat. KCl electrode.

2.3.   Conclusions of section 2

In section 2.1, the author reported that an enzyme-modified electrode was prepared producing a diffusion-limited bioelectrocatalytic current for the reduction of O_2 to water at neutral pH and at ambient temperature. The electrode uses bilirubin oxidase as an enzyme and $[Fe(CN)_6]^{3-/4-}$ as a mediator, both of which are immobilized on the surface of a glassy carbon electrode by electrostatic entrapment with poly-L-lysine. The catalytic limiting current density reached ~2 mA/cm^2 at stirring condition. This modified method can be applied on carbon fiber electrode which electrode surface is large. Plasma treatment can improve the electrode surface to be hydrophobic and make roughness. The catalytic current density of BOD-$[W(CN)_8]^{3-/4-}$-PLL CF fixed disk electrode is about 20-30 mA/cm^2 at 2000 rpm at oxygen saturated conditions. In order to apply this CF electrode to biofuel cell in practical use, enough demand of oxygen and proton is needed unless using oxygen gas flow and pomp system.

In section 2.2, a passive-type air-breathing biocathode derivatized with bilirubin oxidase as enzyme and ferricyanide as redox mediator was investigated. Water repellents from Scotchgard^{TM} with dissolved in methyl isobutyl ketone were directly applied to the enzyme- and mediator-modified biocathode. The partially water-repelled biocathode was placed on a gas-permeable polytetrafluoroethylene (PTFE) membrane and immersed in a buffer solution, and O_2 was passively supplied to the biocathode through the PTFE membrane from air. Cathodic currents were dependent on the buffer concentration and amount of applied water repellent. Steady-state catalytic current densities reached 24 and 32 mA cm^{-2} at 0 V vs. Ag|AgCl under air and oxygen atmospheric conditions, respectively, using a biocathode modified with 0.32 mg cm^{-2} of the water repellent and 2.0 M imidazole buffer at pH 7. Finally, cell power density of the biofuel cell which applied BOD-$[Fe(CN)_6]^{3-/4-}$-PLL CF electrode with water repellent as a biocathode reached 10 mW/cm^2 using previous reported bioanode[23] in passive conditions (Figure 2.12), which are attractive for mobile consumer electronics devices requiring low power less than 100 mW -portable music players.[25]
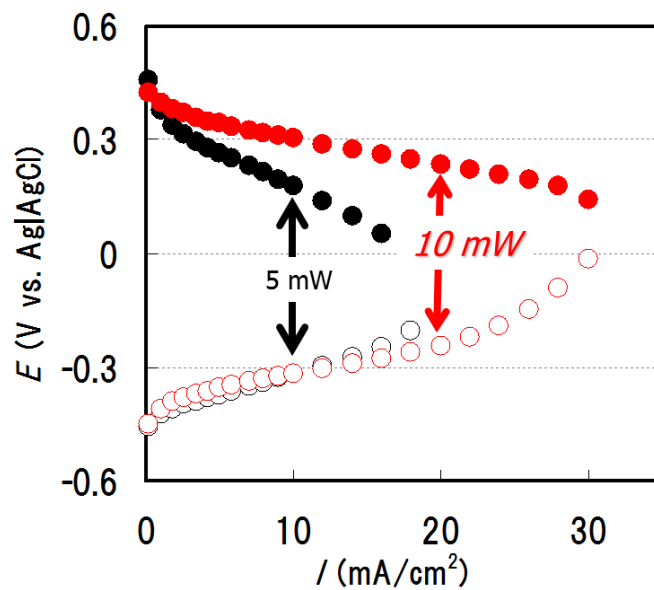
Figure 2.12. Dependence of potential vs. current density of the open-air type biofuel cell (black circles) and biofuel cell using air-breathing biocathode (red circles) in 2.0M imidazole/HCl buffer (pH 7.0) containing 0.4 M glucose. The closed circles show bio-cathode and the open circles show bio-anode.

References and Notes

(1)   Barton, S.C.; Gallaway, J.; Atanassov, P. *Chem. Rev.* **2004**, 104, 4867-4886.

(2)   Willner, I.; Yan, Y.M.; Willner, B.; Tel-Vered, R. *Fuel Cells* **2009**, 9, 7-24.

(3)   Falk, M.; Blum, Z.; Shleev, S. *Electrochim. Acta*, **2012**, 82, 191.

(4)   Leech, D.; Kavanagh, P.; Schuhmann, W. *Electrochim Acta*, **2012**, 84, 223.

(5)   Sakai, H.; Nakagawa, T.; Sato, A.; Tomita, T.; Tokita, Y.; Hatazawa, T.; Ikeda, T.; Tsujimura, S.; Kano, K. *Energy Environ. Sci*. **2009**, 2, 133-138.

(6)   Cracknell, J.A.; Vincent, K.A.; Armstrong, F.A. *Chem. Rev.* **2008**, 108, 2439–2461.

(7)   Meredith, M.T.; Minteer, S.D. *Ann. Rev. Anal. Chem.* **2012,** 5,157–179.

(8)   Tarasevich, M. R.; Bogdanovskaya, V. A.; Gavrilova, E. F.; Orlov, S. B. J. *J. Electroanal. Chem.* **1986,** 206, 217–227.

(9)   Shleev, S.; Tkac, L.; Christenson, A.; Ruzgas, T.; Yaropolov, A.I.; Whittaker, J.W.; Gorton, L. *Biosens. Bioelectron*. **2005**, 20, 2517–2554.

(10)   Hong, G.; Ivnitski, D.M.; Johnson, G.R.; Atanassov, P.; Pachter, R. *J. Amer. Chem. Soc.* **2011,** 133, 4802–4809.

(11)   Tarasevich, M.R.; Yaropolov, A.I.; Bogdanovskaya, V.A.; Varfolomeev, S.D. *Bioelectrochem. Bioener.* **1979**, 6, 393–403.

(12)   Barton, S.C.; Kim, H.-.H.; Binyamin, G.; Zhang, Y.; Heller, A. *J. Amer. Chem. Soc.* **2001**, 123, 5802–5803.

(13)   Tsujimura, S.; Kamitaka, Y.; Kano, K. *Fuel cells*, **2007**, 7, 463–469.

(14)   Ackermann, Y.; Guschin, D.A.; Eckhard, K.; Schleev, S.; Schuhmann, W. *Electrochem. Commun*. **2010,** 12, 640–643.

(15)   Tsujimura, S.; Tatsumi, H.; Ogawa, J.; Shimizu, S.; Kano, K.; Ikeda, T. *J. Electroanal. Chem*. **2001**, 496, 69–75.

(16)   Nakagawa, T.; Tsujimura, S.; Kano, K.; Ikeda, T, *Chem. Lett*. **2003**, 32, 54.

(17)   Mano, N.; Kim, H.-H.; Heller, A. *J. Phys. Chem. B* **2002**, 106, 8842–8848.

(18)   Kamitaka, Y.; Tsujimura, S.; Setoyama, N.; Kajino, T.; Kano, K. *Phys. Chem. Chem. Phys*. **2007**, 9, 1793-1801.

(19)   Kontani, R.; Tsujimura, S.; Kano, K. *Bioelectrochem,***2009,** 76, 10-13.

(20)   Asano, I.; Hamano, Y.; Tsujimura, S.; Shirai, O.; Kano, K. *Electrochem*, **2012**, 80, 324-326.

(21)   Miyake, T.; Haneda, K.; Yoshino, S.; Nishizawa, M. *Biosensors & bioelectronics* **2013**, 40, 45-49.

(22)   Ciniciato, G.P.M.K.; Lau, C.; Cochrane, A.; Sibbett, S.S.; Gonzalez, S.R.; Atanassov, P. *Electrochemica Acta* **2012**, 82, 208-213.

(23)   Sakai, H.; Nakagawa, T.; Mita, H.; Matsumoto, R.; Sugiyama, T.; Kumita, H.; Tokita, Y.; Hatazawa, T. *ECS Transaction* **2009**, 16, 9.

(24)   http://www.mmm.co.jp/scotchgard/products/fabric/

(25)   http://www.sony.co.jp/SonyInfo/technology/technology/theme/bio_01.html

3. Development of functional electrode for electrochemical oxidation of water to oxygen

3.1. Electrogenerated IrO$_2$ nanoparticles as dissolved redox catalysts for water oxidation

3.1.1. Introduction

Using dissolved, freely diffusing molecules as electron transfer mediators is a common tactic in electrochemical redox catalysis.[1,2] Using dissolved, freely diffusing inorganic nanoparticles as electron transfer mediators has seldom been considered, however.[3,4] This paper reports mass transport-controlled Ir$^{V/IV}$ and Ir$^{IV/III}$ voltammetry in pH 13 solutions of Ir^{IV}O$_X$ nanoparticles, and the effectiveness of the Ir$^{VI/V}$ step in the redox catalysis of the oxidation of water (Scheme 3.1). The IrO$_x$ nanoparticles are very small (1.6 $\pm$ 0.6 nm dia., average 66 Ir/nanoparticle, Figure 3.1), and being used in the same medium in which they are hydrolytically prepared,[5] are assumed to be capped solely by hydroxide.   I show that their Ir sites are fully electroactive.
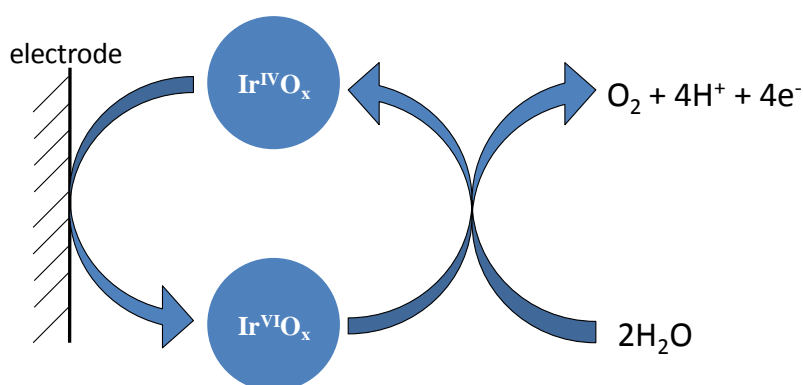
Scheme 3.1. Redox catalysis of water oxidation with dissolved, diffusing IrO$_x$ nanoparticles

3.1.2. Electrochemistry of IrO$_2$ nanoparticles as dissolved redox catalysts for water oxidation

Rotating Pt disk voltammetry (RDE, Figure 3.2) of a pH 13 solution 2.5 mM in Ir^{IV} sites (38 μM in nanoparticles, based on avg. IrO$_x$ nanoparticle size) shows three waves.   Two, with $E^{1/2}$ = -0.62 and 0.25 V, are assigned to Ir$^{V/IV}$ and Ir$^{IV/III}$ oxidation state changes in the nanoparticles, and are mass transport controlled
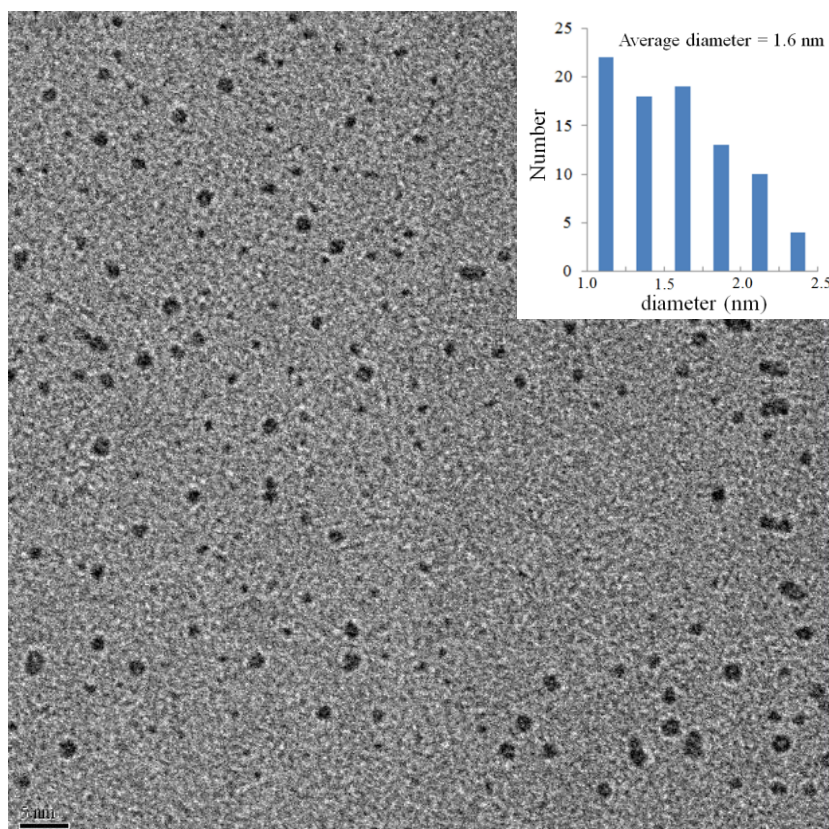
Figure 3.1. TEM image of IrO_x nanoparticles. The average nanoparticle diameter is 1.6 ± 0.6 nm, based on a rutile lattice[14] the average nanoparticle contains 66 Ir sites.

as shown by linear plots of limiting current vs. $\omega^{1/2}$ (inset) and concentration (see Figure 3.3, inset). (RDE currents at intervening potentials are very small, consistent with the nanoparticles being initially in the Ir^{IV} state.) The currents steadily rising beyond the $Ir^{V/IV}$ wave plateau (from ca. +0.45 V) reflect electrochemical generation of Ir^{VI} states in the nanoparticles that act as redox catalysts for the $H_2O \rightarrow O_2$ oxidation (Scheme 3.1). Currents in this $4e^-$ catalytic wave, while proportional to nanoparticle concentration (Figure 3.3, inset), are nearly independent of ω (Figure 3.2 inset, Δ), which clearly signifies a rate-limiting reaction step in the nanoparticles' reaction(s) with water.[6a] Rotating ring-disk electrode (RRDE) results show that $Ir^{VI}O_X$ nanoparticles electrogenerated at +1.0 V (Figure 3.4) and at +0.55V (Figure 3.5) produce O_2 with 100 % efficiency. (In the RRDE experiment, O_2 produced by Scheme 3.1 near the disk is swept to the ring electrode and reduced in a $2e^- : O_2 \rightarrow H_2O_2$ wave.) Based on the ratio of O_2 ring to catalytic disk currents, the observed collection efficiency N/2 exactly matches the 11 % expected from the RRDE geometry (see Figure 3.4 caption).
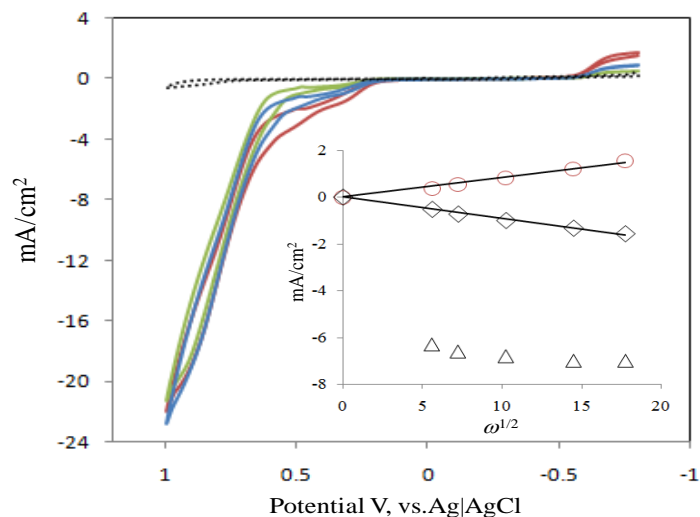
Figure 3.2. RDE (Pt disk) of deaerated pH 13 IrO_x nanoparticle solution (2.5 mM in Ir sites) at electrode rotation rate ω = 300 (ocher), 1000 (blue) and 3000 rpm (red). The dashed black line is RDE in nanoparticle-free deaerated pH 13 solution at 300 rpm. Potential scan rate 20 mVs^{-1}. Insert shows Levich plots at -0.8 V (circle, $Ir^{IV/III}$ wave), 0.4 V(diamond, $Ir^{V/IV}$ wave) and 0.7 V (triangle, water oxidation by Ir^{VI}).

That is, the redox catalysis reaction of Scheme 3.1 quantitatively converts oxidative charge delivered to the nanoparticle mediators to the production of O_2. This first electrochemical demonstration of water oxidation mediated by dissolved nanoparticles opens up study of the water oxidation reaction (kinetics and mechanism) by manipulation of solution and transport parameters that would be less readily controlled or ascertained were the nanoparticles coated onto the electrode in an electrocatalytic film.

Indeed, the author reported[5] the electrocatalysis of water oxidation by films of similarly prepared IrO_X nanoparticles that were electroflocculated onto electrodes, and which display catalytic properties similar to those the author report here for the dissolved IrO_X nanoparticles (see Figure 3.6).   Thus, at 100% current efficiency and 0.5 mA/cm^2, both film[5] and dissolved nanoparticles[6b] exhibit η = 0.29 V. The film and dissolved nanoparticle η results both surpass previous recent descriptions of electrocatalytic water oxidation (at the same current density), by films on ITO electrodes (50-100 nm dia. citrate-stabilized IrO_2 nanoparticles, $\eta \approx 0.42$ V, pH 5.3) [7], and by films containing Co^{2+} and phosphate ($\eta \approx 0.5$ V , pH 7).[8]
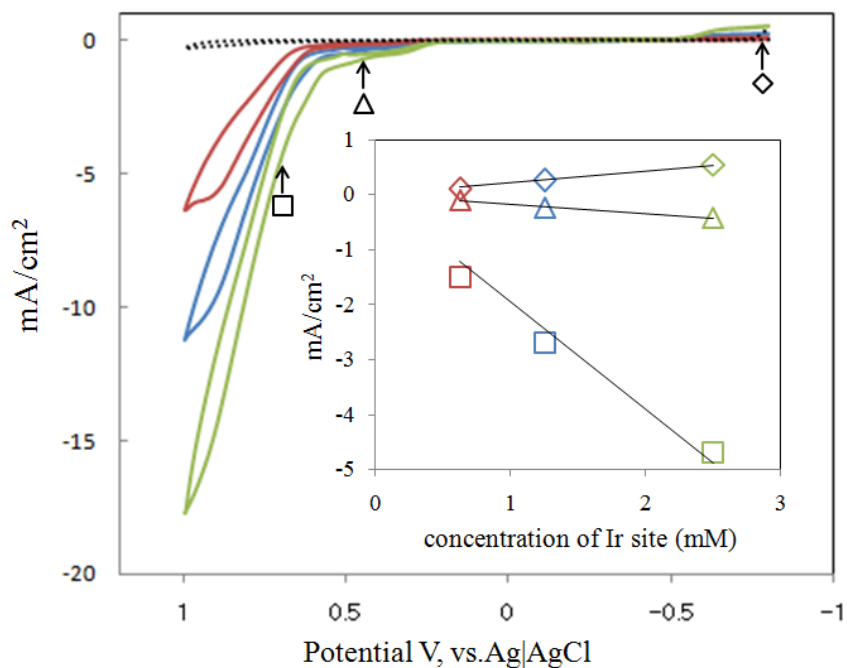
[Ir site]	$I_{0.4V}$ (mAcm^{-2})	$I_{1.0V}$ (mAcm^{-2})	$I_{1.0V}/I_{0.4V}$	turnover
0.63 mM	0.14	6.1	44	11
1.25	0.27	11.0	41	10
2.5	0.51	17.7	35	8.7

Figure 3.3. Rotating (Pt) Disk Voltammetry (RDE) of Ir^{IV}O$_x$ nanoparticle solution at 300 rpm and 20 mVs^{-1} scan rate, (showing forward and reverse scans).   The pH 13 solution contains 0.63 (red), 1.25 (blue) and 2.5 mM (ocher) iridium sites. The 0.63 and 1.25 mM solutions were diluted from the 2.5 mM solution, whose concentration is based on the Ir content of the IrCl$_6^{2-}$ solution that was hydrolyzed to produce the nanoparticles. Insert shows the current density dependence on Ir concentration at -0.8 V (diamond), 0.4 V(triangle) and 0.7 V (square).   The table shows the ratio of currents at +1.0 V (four electrons/Ir and Scheme 3.1 regeneration, $\eta = 0.74$ V) to those at +0.4 V (one electron, Ir$^{V/IV}$, and no regeneration) which gives the Ir site TO, which is independent of nanoparticle concentration.

Another comparison of film and dissolved nanoparticles as catalysts is based on Ir site turnover frequency (TO, mol O$_2$/Ir sites/sec).   To make this comparison, conditions for the dissolved nanoparticles were selected that demonstrably (see Figure 3.7) avoid their electroflocculation[5] and consequent artifactual electrocatalysis by a nanoparticle film (e.g., the currents are due solely to diffusing nanoparticles.)   In RDE voltammetry, the turnover (TO) frequency of iridium sites in dissolved IrO$_X$ nanoparticles at 1.0 V and 300 rpm was estimated as 8-11 s^{-1} based on the ratio of currents at +1.0 V (four electrons/Ir and Scheme 3.1

45

regeneration, $\eta = 0.74$ V) to those at +0.4 V (one electron, $Ir^{V/IV}$ reaction, and no regeneration). The TO rate is independent of nanoparticle concentration (see Figure 3.3), and is nearly the same as that (6 s^{-1}) measured[5] for films of electroflocculated IrO_X nanoparticles. This result, that surface electrocatalysis and solution redox catalysis can show identical kinetics, is in fact consonant with expectations1 of chemically modified electrodes when the current is neither electron or mass transport but reaction rate limited.

The Ir sites in the nanoparticles are exhaustively electroactive, as shown by controlled potential coulometry (Figure 3.8a). The collected charge for $Ir^{IV} \rightarrow Ir^{III}$ conversion was 96 % of the Ir site concentration known to be present in the solution from the hydrolytic synthesis from $IrCl_6^{2-}$. This complete reactivity contrast with previous experiments on Ir oxide films[9] and 50 nm nanoparticle films,[7] where only a small fraction (3.7 % and 1 6%, respectively) of the total Ir sites were electroactive. This seems clearly to be a nanoparticle size effect, wherein the very small electron and proton transport distances enable complete Ir site reactivity.
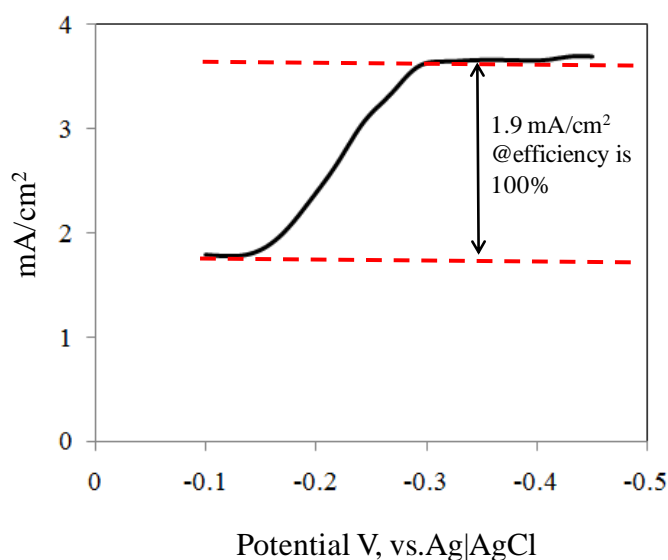
Figure 3.4. RRDE Experiment. Oxygen reduction wave at Pt ring electrode (300 rpm) while Pt disk maintained at +1.0V, in pH 13 deaerated IrO_x nanoparticle solution ([Ir] = 2.5 mM). Potential scan rate 5 mVs^{-1}). (During the scan, disk current decreased slightly (-17.1 to -16.3 mAcm^{-2}). Ratio of ring to disk currents gives collection efficiency (N/2) of 11 %, which accounting for disk (4e) and ring (2e) reactions and calibrated N of 22 %, corresponds to 100 % current efficiency for water oxidation to O_2.
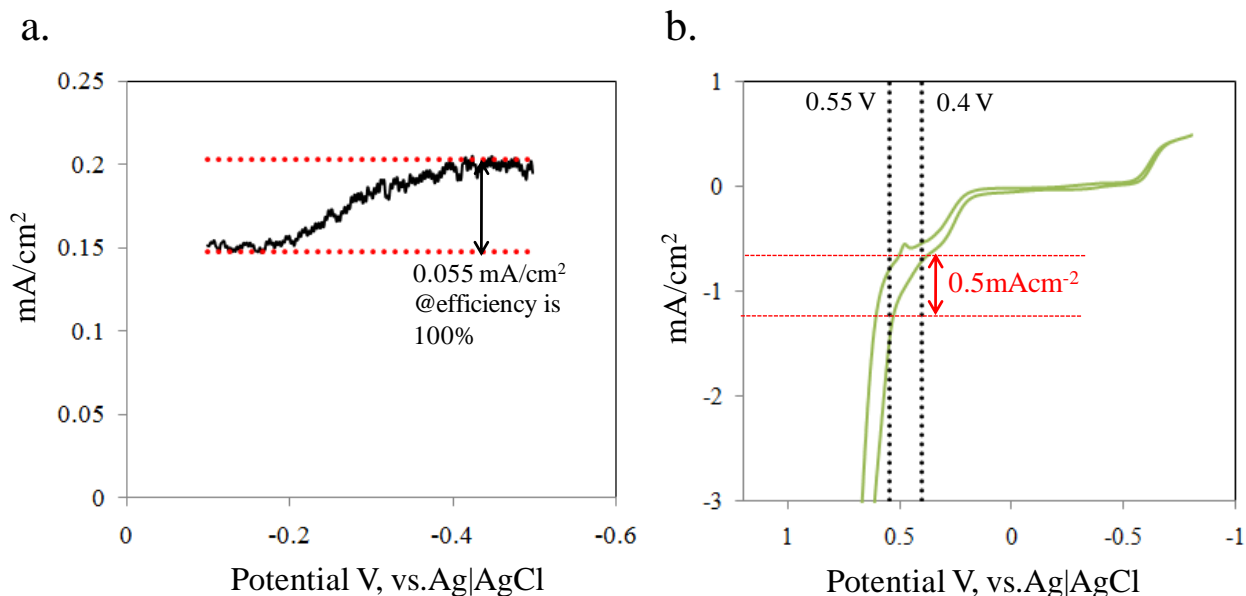
Figure 3.5. Rotating ring disk electrode (RRDE) experiments. (a) Current-potential response for the reduction of O_2 (as in Figure 3.4) at Pt ring from -0.1 V to -0.5 V (black line) in deaerated IrO_x nanoparticle solution at 300 rpm ([Ir] = 2.5 mM, pH 13, potential scan rate 20 mVs^{-1}) and disk potential of 0.55 V (η = 0.29 V). Subtracting the current for the $Ir^{V/IV}$ wave using its plateau at +0.4V (see Panel (b)) from the current at Pt disk electrode at 0.55 V gives a net catalytic current density of about 0.5 mA cm^{-2}. Based on the ratio of the latter result and the limiting current for the O_2 wave in Panel (a), the collection efficiency (N/2) is 11 % which corresponds to 100% current efficiency for O_2 generation at +0.55V. (During the -0.1 V to -0.5 V ring electrode scan, the current density at Pt disk at 0.55 V decreased slightly (-1.18 to -1.03 mA cm^{-2}); the average was taken to calculate the N/2 value.) (b) RDE voltammetry (showing forward and reverse scans) of deaerated IrO_x nanoparticle solution (2.5 mM in Ir) at pH 13 using Pt disk electrode at 300 rpm.

The similarity of η and TO for electroflocculated and dissolved IrO_X nanoparticles supports our previous[5] assumption of exhaustively electroactive Ir sites in the nanoparticles comprising the electroflocculated films.

3.1.3. Electrochemical analysis of electro-active Ir atom of IrO_2 nanoparticles

The voltammetry of the dissolved IrO_X nanoparticles at lower potentials is well-defined, as seen by RDE in Figure 3.2, inset and by CV in Figure 3.8b. The waves in the diffusion controlled CV, assigned to $Ir^{V/IV}$ and $Ir^{IV/III}$ reactions, are quasi-reversible (ΔE_{PEAK} = 70 mV) with formal potentials at $E^{o'}$ = -0.62 V and 0.25 V, agreeing with RDE observations (Figure 3.2).
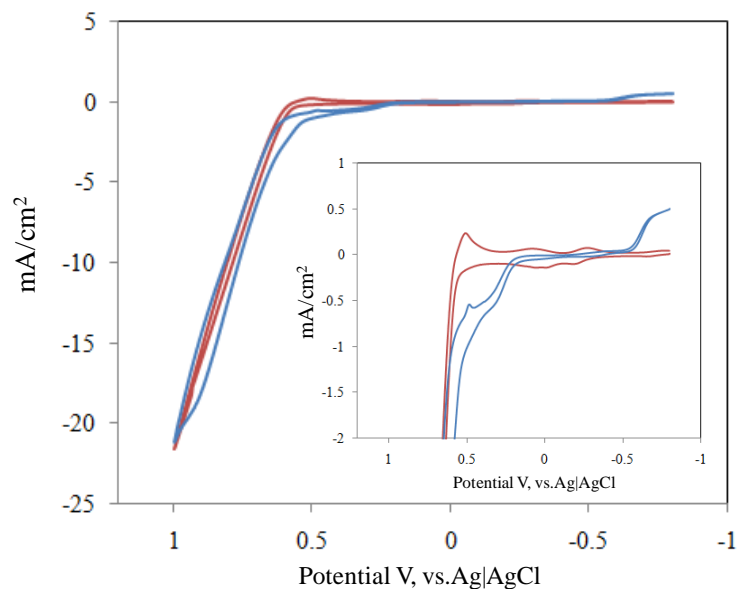
Figure 3.6. RDE voltammetry of film of electroflocculated IrO_x on glassy carbon electrode in nanoparticle-free pH 13 solution (red line, $\Gamma_{Ir} = 7.0 \times 10^{-9}$ mol/cm^2), and of naked Pt electrode in deareated nanoparticle solution at pH 13 (blue line, [Ir] = 2.5 mM) (showing forward and reverse scans). $\omega = 300$ rpm. Γ_{Ir} measured as in Ref. 5.
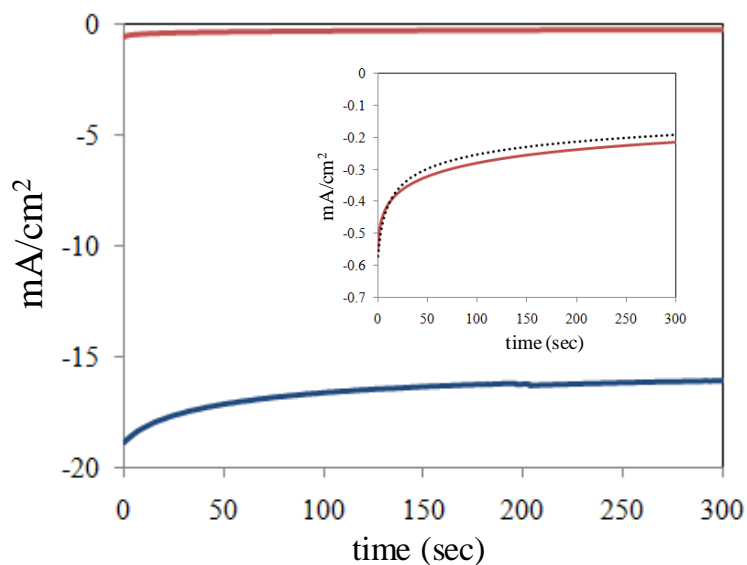
Figure 3.7. Current-time at RDE (platinum disk electrode, $\omega = 300$ rpm) for applied potential at 1.0 V in IrO_x nanoparticle solution (total [Ir] site concentration = 2.5 mM, pH 13) (blue line). After the blue line experiment, the RDE is rinsed and transferred to nanoparticle-free pH 13 solution (0.1 M NaOH). Application of 1.0V to the RDE gave much smaller currents (red line) that were close to currents observed at a freshly polished RDE electrode (black dash line) in the same nanoparticle-free pH 13 solution. Inset shows the red and black dashed lines magnified. The similarity of the red and dashed black line current responses is evidence that no significant electro-flocculation of nanoparticles onto the electrode occurred. The reason(s) for the modest decrease with time of O_2 evolution current (blue line) are presently unclear.
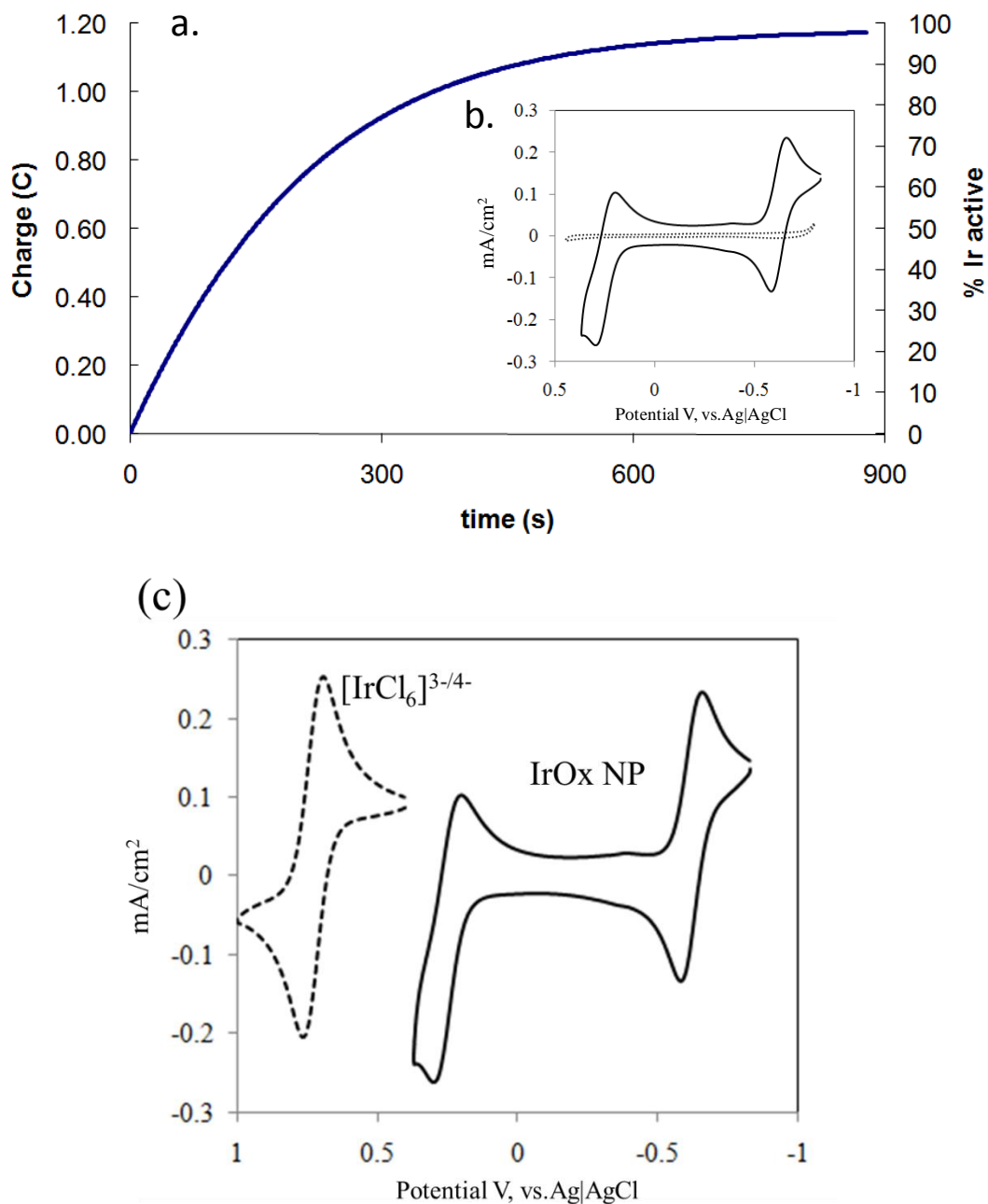
Figure 3.8. (a) Controlled potential coulometry on 5 mL of deaerated IrO_2 nanoparticle solution (containing 12.5 mmole iridium site) at pH 13 using platinum mesh electrode with stirring. The potential step is from -0.45V to -0.75V. The current is reduction Ir^{IV} to Ir^{III}. (b) CV of deaerated IrO_2 nanoparticle solution where [Ir] =2.5 mM (black line) and control CV (dashed black line). pH 13, Pt disk electrode, scan rate 20 mVs^{-1}. (c) CVs of deaerated IrO_2 nanoparticle solution (a solid line) and $[IrCl_6]^{3-/4-}$ (dash line) where [Ir] =2.5 mM at pH 13, Pt disk electrode, scan rate 20 mVs^{-1}.
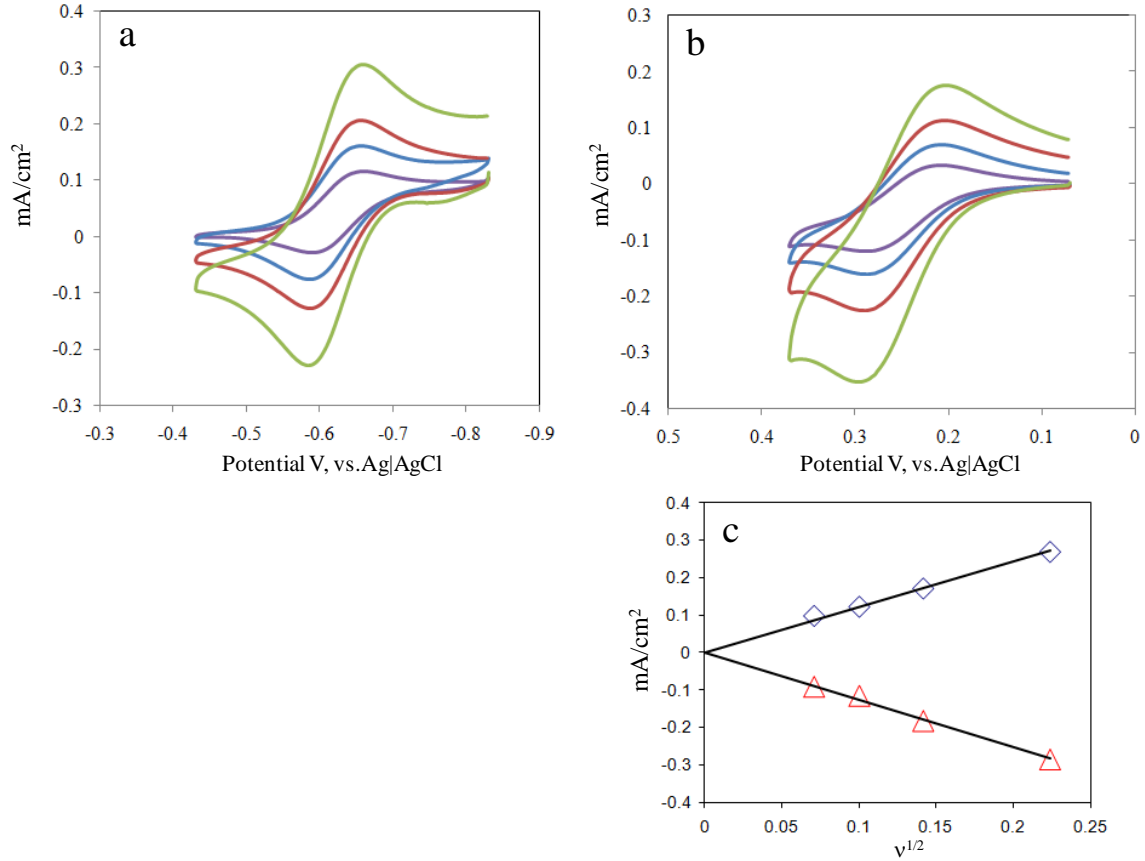
Figure 3.9. Cyclic voltammetry in unstirred solutions of deaerated $Ir^{IV}O_x$ nanoparticles ([Ir] = 2.5 mM) at pH 13. Panels (a) $Ir^{IV/III}$ and (b) $Ir^{V/IV}$ waves at potential scan rates 5, 10, 20 and 50 mVs^{-1}. Panel (c) Nanoparticle peak current densities from Panels (a) (blue) and (b) (red) vary linearly with square root of scan rate. The ΔE_{peak} of each wave is 70 mV at 20 mVs^{-1}.

These potentials is completely different from the redox potencial of $[IrCl_6]^{3-/4-}$ in spite of both peak current is almost same value at same pH condition (Figure 3.8c). This indicates that electron transfer between dissolved IrO_X nanoparticles and electrode surface is as fast as that of $[IrCl_6]^{3-/4-}$.

The nanoparticle diffusion coefficient was calculated from CV peak currents (See Figure 3.9) and Levich plots (Figure 3.2, insert) using

$$i_{PEAK} = 2.69 \times 10^5 n^{3/2} A D^{1/2} v^{1/2} C_{Ir} \qquad (3.1)$$

$$i_{LIM} = 0.62 n F A D^{2/3} v^{-1/6} \omega^{1/2} C_{Ir} \qquad (3.2)$$

where n = 1 and C_{Ir} = Ir site concentration, following previous multi-electron transfer work[13] on dissolved, diffusing redox polymers. The results, $D = 3.3 \times 10^{-6}$ and 4.0×10^{-6} cm^2/s, respectively, are consistent

50

with the prediction, 3.1 ($\pm$1.9)$\times 10^{-6}$ cm^2/s, of the Einstein-Stokes equation for a 1.6 ($\pm$0.6) nm nanoparticle,

$$D = kT/6\pi\eta r \qquad\qquad (3.3)$$

The diffusing IrO$_X$ nanoparticles seem well behaved as multi-electron electroactive species, which is a favorable portent for application of voltammetric mass transport principles to more deeply probe theirreactivity properties with water and other species.

3.1.4. Conclusions

In conclusions, I describe the electrochemical properties of 1.6 $\pm$ 0.6 nm IrO$_X$ nanoparticles in aqueous solution. The nanoparticles' Ir$^{IV/III}$ and Ir$^{V/IV}$ reactions proceed at mass transport-controlled rates, and are quasi-reversible. Bulk electrolysis reveals exhaustive electrochemical reactivity of the Ir nanoparticle sites, which I attribute to the small nanoparticle size allowing adequate electron and proton transport throughout. When driven to the Ir^{VI} state, the nanoparticles oxidize water to O$_2$ at 100% current efficiency at over-potentials as small as 0.29 V.

3.1.5.   Experimental

K$_2$IrCl$_6$ (99.99%) and NaH$_2$PO$_4$ (99%) were purchased from Aldrich and Sigma-Aldrich, respectively. IrO$_x$ nanoparticle was prepared from 2.5 mM aqueous K$_2$IrCl$_6$ adjusted to pH 13 with NaOH (25 w/v%), heated at 90°C for 20 min, and immediately cooled in an ice-bath, producing a blue solution (optical absorbance peak at 582 nm, Ir^{IV}O$_x$) containing well dispersed, stable 1.6 nm dia. nanoparticles (Figure 3.1) that remained unchanged for >2 months at pH 13 in a refrigerator. Electrochemical measurements were carried out on a Bioanalytical Systems (BAS) 100B electrochemical analyzer and CH instrument analyzer for RRDE experiment. A platinum mesh electrode was used in the coulometry experiment.

Modulated Speed electrode rotator was AFMSRCE and electrode was E7R8, Pt flag counter electrode, and Ag/AgCl reference electrode, all from Pine Research Instrumentation, Inc.. The surface areas of platinum disk and platinum ring electrodes are 0.164 and 0.036 cm^2, respectively. The water oxidation reaction on IrO_x solution involves four electrons while oxygen reduction on the Pt electrode involves two electrons, so the calibrated 22 % RRDE collection efficiency N is divided by two. The collection efficiency of oxygen evolution observed at pH 13 is 11 % as shown in Figures 3.4. When detecting oxygen generated at the RRDE disk, the solution was first deareated with bubbling Ar for 1 hour. TEM samples were prepared by placing a droplet containing IrO_x nanoparticles onto a copper grid (200 copper mesh; carbon-coated Formvar). TEM images were obtained on a JEOL 2010F FasTEM.

References and Notes

(1)   Savéant, J-M. *Chem. Rev.* **2008**, 108 (7), 2348-2378

(2)   Cracknell, J. A.; Vincent, K. A.; Armstrong, F. A. *Chem. Rev.* **2008**, 108 (7), 2439-2461

(3)   Miller, D. S.; Bard, A. J.; McLendon, G.; Ferguson, J. *J. Am. Chem. Soc.* **1981**, 103, 5336.

(4)   Xiao, X.; Fan, F-R, F.; Zhou, J. and Bard, A.J. *J. Am Chem. Soc.* **2008**, 130, 16669–16677.

(5)   Nakagawa, T.; Christopher, B.A.; Murray, R.W. *J. Phys. Chem. C* **2009**, 113, 12958–12961.

(6)   (a) Linear Koutecky-Levich plots for the slight dependency on ω of currents at +0.7V in Figure 3.2 inset are undergoing further analysis. (b) The dissolved nanoparticle η value corresponds to the result at +0.55V (Figure 3.5) demonstrating O_2 production at 100% current efficiency.

(7)   a) Yagi, M.; Tomita, E.; Sakita, S.; Kuwabara, T.; Nagai, K. *J. Phys. Chem. B* **2005**, 109, 21489. b) Kuwabara, T.; Tomita, E.; Sakita, S.; Hasegawa, D.; Sone, K.; Yagi, M. *J. Phys. Chem. C* **2008**, 112, 3774-3779

(8)   a) Kanan, M.W.; Nocera, D. G. *Science* **2008**, 321, 1072. b) Surendranath, Y.; Dincă, M., Nocera, D.G. *J. Am. Chem. Soc.* **2009**, 131, 2615.

(9)   Fierro, S.; Nagel, T.; Baltruschat, H.; Comninellis, T. *Electrochem. and Solid-State Lett.* **2008**, 7, E20-E23.

(10)   Brewer, S.H.; Wicaksana, D.; Maria, J-P.; Kingon, A. I.; Franzwz, S. *Chem. Phys.* **2005**, 313, 25.

(11)   Chen, Y.; Shi, P.; Scherson, D. *Electrochemical and Solid-State Letters*. **2008**, 11, F5

(12)   Comninellis, Ch.; Vercesi, G. P. *J. Appl. Electrochem.* **1991**, 21, 335.

(13)   Flanagan, J. B.; Margel, S.; Bard, A. J.; Anson, F. C. *J. Am. Chem. Soc.* **1978**, 100, 4248-4253.

(14)   El Khakani, M. A.; Chaker, M.; Gat, E.   *Appl. Phys. Lett.*, **1996,** *69,* 2027.

3.2. Efficient electro-oxidation of water near its reversible potential by a mesoporous IrO_2 nanoparticle film

3.2.1. Introduction

Energy systems that are eco-friendly emphatically include the exploitation of solar energy in photoelectrochemical cells to split water into O_2 and H_2, the energy-producing recombining of which is carbon neutral. Of the many components of water-splitting solar cell design, that of the electrocatalytic oxidation of water to O_2

$$2H_2O \rightarrow 4H^+ + O_2 + 4e^- \qquad (3.4)$$

is recognized [1-3] as a potential bottleneck because of its slow electrode kinetics. While an ideal electrocatalytic process would drive reaction (3.4) at its thermodynamic potential (for example, at 0.62 V vs. Ag/AgCl, at pH 7 and 1 atm O_2), the actual electrode reaction occurs at a more positive potential (an "over-potential", η) whose magnitude reflects the electrode kinetics. Over-potentials cause a partial loss of photon energy (typically harvested by a dye's absorption and subsequent electron transfers). The loss can be substantial—for example $\eta = 0.5V$ is 40% of the 1.23 V thermodynamic potential required to split water. Since larger applied over-potentials enhance the reaction rate (electrochemical current), η is customarily stated for a specified current. In practice, one seeks electrocatalysis in which modest values of η yield significant O_2-evolving currents for reaction (3.4).

This paper reports progress in this direction by achieving the smallest electrochemical η value yet reported for reaction (3.4), using as catalyst a stable, adherent, mesoporous film containing 1.6 nm dia. $Ir^{IV}O_x$ nanoparticles. Demonstrable O_2 evolution is electrochemically initiated at $\eta =$ only ~0.15 V higher than the reversible H_2O/O_2 potential and achieves 100 % current efficiency (0.5 mA/cm^2 rate) at ~0.25 V. The η is furthermore independent of pH, from 1.5 to 13. At a much larger η (0.68 V), the O_2 evolution rate becomes large, nearly 0.1 A/cm^2.

Certain metal complexes, Ir and Ru in particular,[4-7] raised to high oxidation states are known catalysts for water oxidation. Metal oxides at high valency also show interesting activity as water oxidation catalysts, including RuO_2, IrO_2, Co_3O_4, Rh_2O_3 and Mn_2O_3.[2,8-10] Harriman[8] showed that high valent states of citrate-stabilized IrO_2 particles actively oxidize water. Mallouk[2], in an elegant photochemical water oxidation scheme, successfully used electron transfers to adsorbed, photogenerated $[Ru(bpy)_3]^{3+}$ to oxidatively charge 2 nm butylmalonate-stabilized IrO_2 nanoparticles. Yagi[10] showed that 50-100 nm dia. citrate-stabilized IrO_2 nanoparticles spontaneously adsorb on ITO electrodes; about 16 % of the Ir sites in the resulting films are active water oxidation catalysts at +1.3 V vs. Ag/AgCl (η = 0.58 V , pH 5.3) at an avg. turnover (TO) frequency, mol O_2/mol Ir, of ~6.6 sec^{-1} (23,600 h^{-1}). Using a different approach, Nocera[1] reports that films containing Co^{2+} and phosphate deposited onto ITO electrodes electrochemically oxidize water at pH 7. These important reports[1,10] provide existing electrocatalysis benchmarks for efficacy (small η) of water oxidation of η = 0.410 and 0.5V[1] at respectively, pH 5.3 and 7, expressed at a common (0.5 mA/cm^2 rate) current density.

3.2.2. Electrochemical oxidation of water by mesoporous IrO₂ nanoparticle film

The work described here uses conductive [11-14] films of IrO_x nanoparticles (~1.6 nm dia., see Figure 3.10a,c) prepared by thermal hydrolysis of K_2IrCl_6 at pH 13 and without addition of stabilizer ligands, producing a clear blue solution (stable to refrigerator storage for > 2 months)[15]. Films of nanoparticles were electro-flocculated onto a glassy carbon electrode (GC, 3 mm dia.) at +1.3 V vs. Ag/AgCl.

After 10 min, the current has increased to > 15 mA/cm^2, and is noisy (Figure 3.11) owing to the copious O_2 gas evolution. It is well-known[13] that the electrochemical properties of IrO_x films can be strongly dependent on the method of film preparation, so it is important to note that forming IrO_x films by electro-flocculation is previously unreported.The substrate electrode can be ITO, platinum or gold. The nanoparticle film thickness can be manipulated by the duration of the electro-flocculation deposition and the IrO_x nanoparticle solution concentration. That the mechanism of IrO_x nanoparticle film formation is electro-flocculation, as opposed to aggregation (in which particle sizes increase), was established by
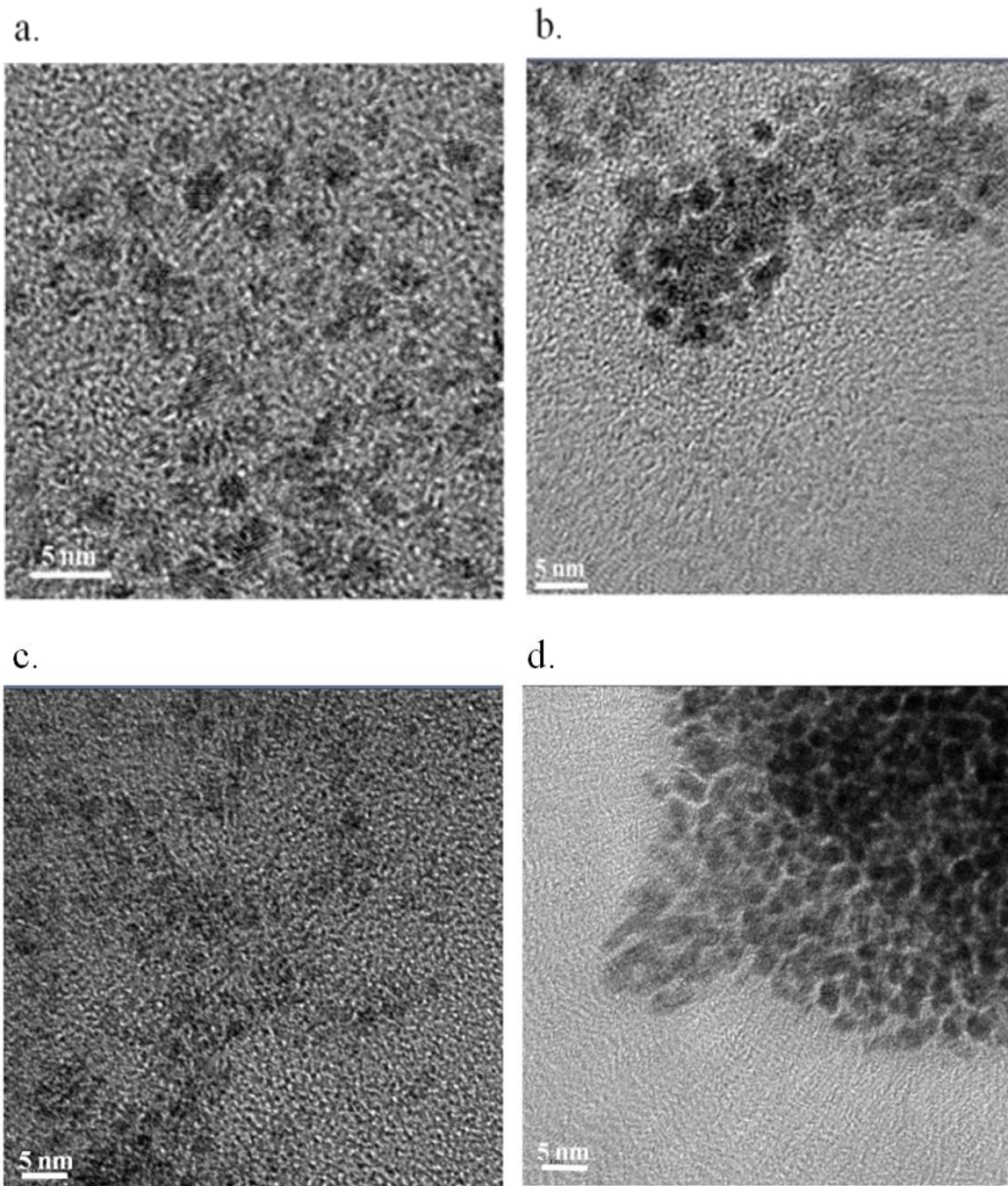
Figure 3.10. (Panel a) TEM image of film of IrO_x nanoparticles cast from their synthesized solution (at pH 13). (Panel b) The IrO_x nanoparticles in the synthesized solution precipitate as an agglomerated mass if the solution is lowered from pH 13 to pH 7 by adding HCl. Many ca. 1.6 nm nanoparticles can still be perceived in the precipitated mass. (Panel c) If 1.0 M phosphate is added to the pH 13 synthesized solution before adjusting to pH 7 by adding HCl, neither precipitation or aggregation of the IrO_x nanoparticles occurs. (Panel d) TEM of mass of IrO_x nanoparticles ultrasonically dislodged from an electro-flocculated nanoparticle film. The image shows that the nanoparticles, after flocculation, are still ca.1.6 nm nanoparticles (like those in the synthesized, deposition solution) and have not undergone aggregative size increase (i.e., have flocculated, not aggregated).
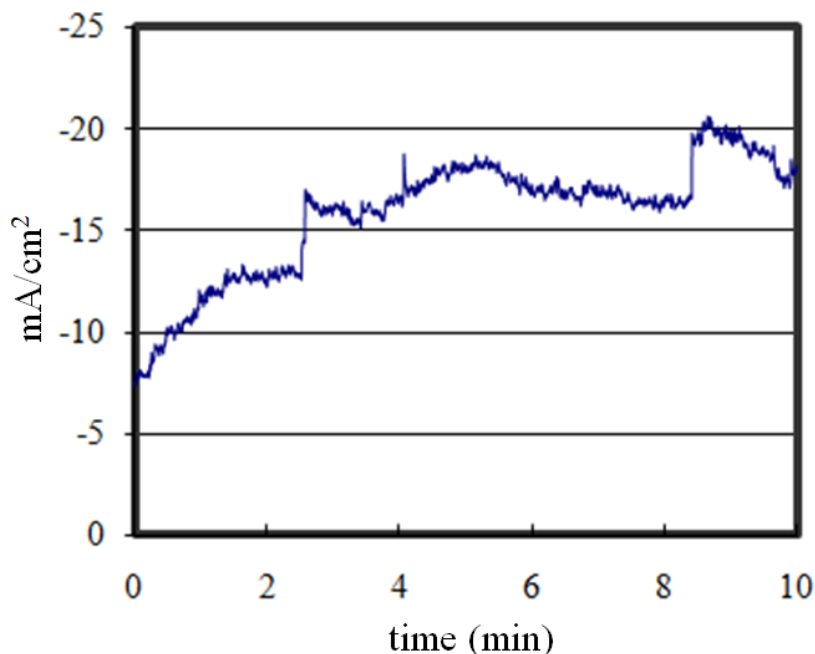
Figure 3.11. Electrocatalytic currents for water oxidation increase with time in pH 13 solution during electro-flocculation of a film of IrO$_x$ nanoparticles.

dis-lodging some of the nanoparticle film from the electrode by prolonged sonication in a nanoparticle-free pH 13 solution. TEM of dislodged fragments (Figure 3.10d) shows that the nanoparticles comprising the film have retained their original ca. 1.6 nm diameter. I consider that during electro-flocculation at pH 13, protons released by water oxidation lower the local pH at the electrode surface so as to partly neutralize the nanoparticle hydroxyl capping layer that had served to stabilize and solubilize the IrO$_x$ nanoparticles. Indeed, lowering the pH of the pH 13 synthesized IrO$_x$ solution by HCl addition causes formation of a precipitate which by TEM (Figure 3.10b) retains large numbers of ca. 1.6 nm dia. nanoparticles. The occurrence of electro-flocculation depends on causing water oxidation at currents above ~0.1 mA/cm^2.
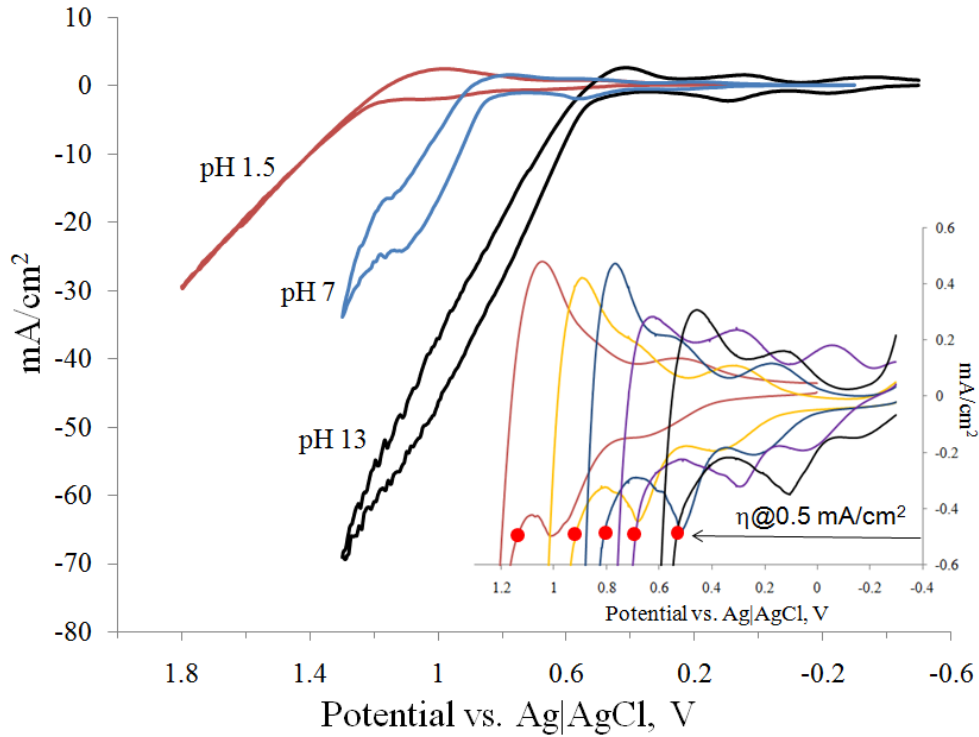
Figure 3.11. Cyclic voltammogram (20 mVs^{-1}) of electro-flocculated IrO$_x$ nanoparticle film on GC electrode at pH = 1.5 (red), 5 (yellow), 7 (blue), 10 (purple) and 13 (black).   pH 5, 7 and 10 solutions contain 1.0 M phosphate buffer; pH 1.5 and 13 only H$_2$SO$_4$ or NaOH. Γ_{Ir} = 7.8$\times$10^{-8} mol/cm^2 but for inset, Γ_{Ir} = 1.6$\times$10^{-8} mol/cm^2.
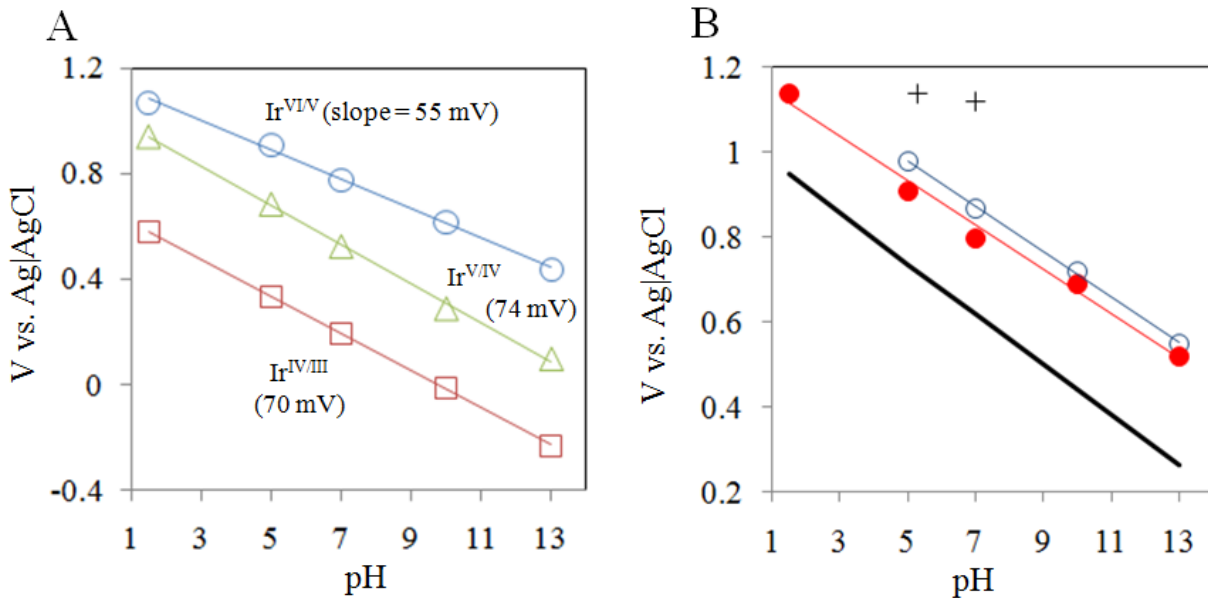
Figure 3.12. (A) pH dependence of Ir$^{III/IV}$(red square), Ir$^{IV/V}$(ocher   triangle) potentials and of anodic peak of Ir$^{VI/V}$ (blue circle); (B) pH dependence of thermodynamic potential for H$_2$O/O$_2$ (black), over-potentials η for initiating water oxidation at 0.5 mA/cm^2 (red, from red • in Figure 3.11) and (blue circle) potential at which conversion to oxygen = 100 % (Figure 3.17). + points shows previous results (refs 1,10).

58

The IrO$_x$ nanoparticle film is stably adherant; the coated GC electrode can be rinsed with water and used in nanoparticle-free solutions for further water oxidation experiments, at any pH. Figure 3.11 shows voltammetry at different solution pH. The sharply rising anodic currents at high potentials (towards the left) correspond to quantitative O$_2$ evolution (as demonstrated below). The potentials for onset of O$_2$ evolution at a 0.5 mA/cm^2 rate and 100% current efficiency (see solid red • in Figure 3.11, inset) are compared at different pH values in Figure 3.12B to the thermodynamic potentials for reaction (3.4). The experimental results give a nearly pH-independent over-potential (η) for water oxidation of $\approx$ 0.25 V (avg.). The current at which η is measured was chosen as the same used in the previous reports.[1,10] The results show that η for water oxidation on the IrO$_x$ nanoparticle film electrode has been brought substantially closer to the reversible potential for water oxidation than previous benchmark efforts (see + points, Figure 3.12B).
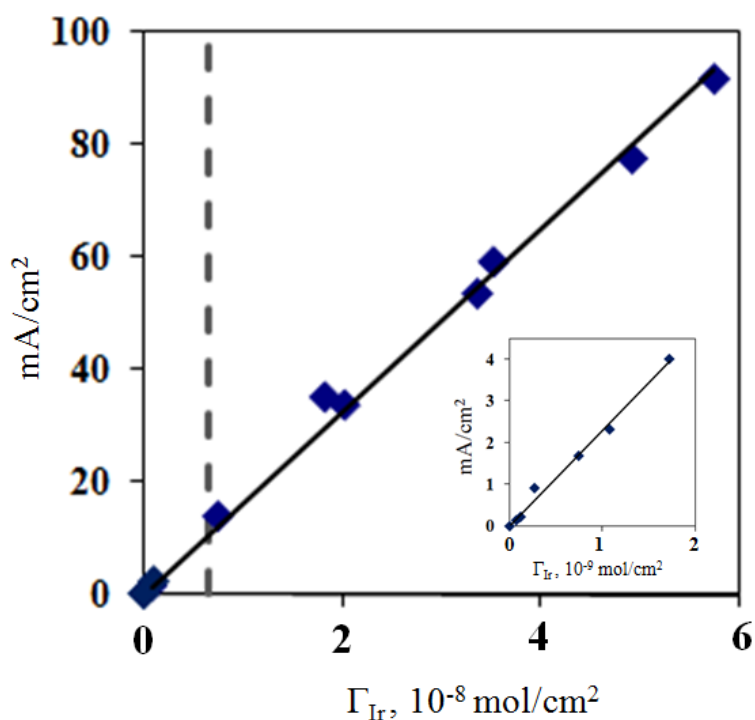
Figure 3.13. Dependence of steady state current density after 150 sec with stirring at 1.3 V vs. Ag/AgCl, vs. coverage Γ_{Ir} of electroactive IrO$_x$ nanoparticle sites, as measured from the Ir^V/Ir^{IV} wave, for films flocculated onto GC electrode, in 1.0 M phosphate buffer (pH 7). Vertical dashed line is Γ_{Ir} corresponding to a IrO$_x$ nanoparticle monolayer.

A.
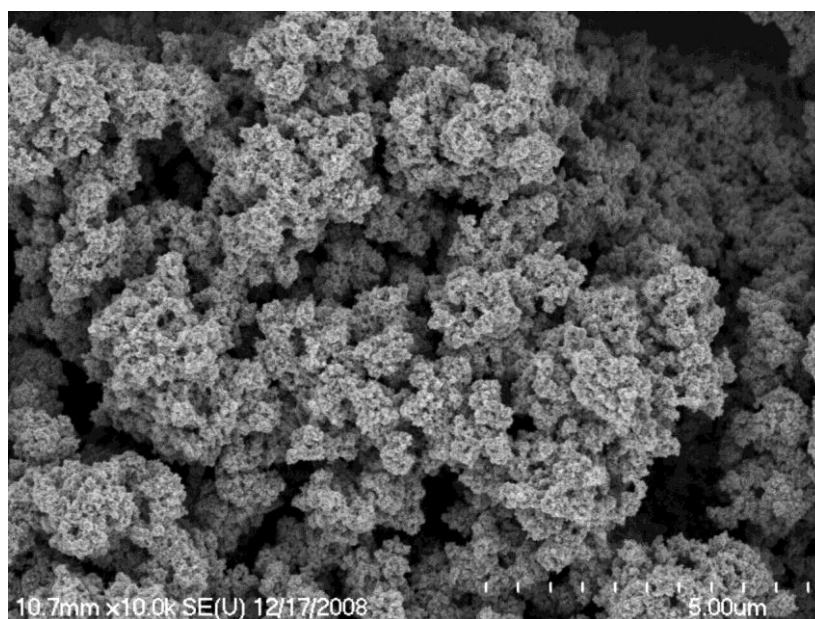
B.
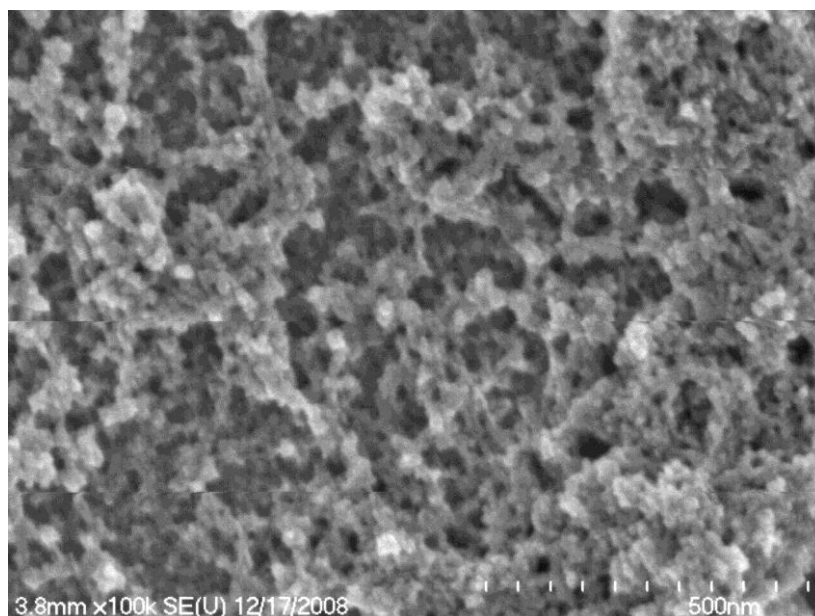
Figure 3.14. Scanning Electron Microscopy (SEM) image of IrO_x nanoparticle film electro-flocculated onto ITO electrode. Following electro-flocculation on the ITO electrode, the nanoparticle films were rinsed with deionized water and allowed to dry in air before loading into the instrument. The images show that the films are highly porous. The overall thickness tends to be uneven, and sometimes uncovered ITO is visible (by EDX).

The author additionally find that the nanoparticle stabilizing ligand must play a role in the efficiency of water oxidation at the nanoparticle/solution interface, since butylmalonate-stabilized[2] nanoparticles produced relatively weak water oxidation electrocatalysis.[16]

The voltammetric waves in Figure 3.11 (see inset), at potentials less high than those causing water oxidation, have (at pH 7) formal potentials of +0.2 V and +0.53 V vs. Ag/AgCl. These waves are assigned, respectively, to Ir^{IV}/Ir^{III} and Ir^{V}/Ir^{IV} redox steps in the IrO_x nanoparticle film, following previous work.[10,11,13] The peak seen on the reverse potential scan at ~ +0.78 V vs. Ag/AgCl (at pH 7) is attributed to reduction of film Ir^{VI} states not yet consumed by water reaction; this peak's potential gives a rough measure of the Ir^{VI}/Ir^{V} potential. The potentials of the Ir^{IV}/Ir^{III} and the $Ir^{V}/^{IIV}$ nanoparticle couples, and of the η for O_2 evolution onset,[17] all shift by ~0.06 V/pH unit (Figures 3.12A and 3.12B, respectively). The author interpret the pH dependency as meaning that the reactions all involve one e^-/one H^+ steps that are relatively fast (ca. Nernstian) and precede the kinetically limiting culmination of O_2 release at the Ir^{VI} state.

The charge under the Ir^{V}/Ir^{IV} wave (Figure 3.11) was used to estimate the population of electroactive IrO_x sites in the nanoparticle film (Γ_{Ir}, mol/cm^2), with results in Figure 3.13. Γ_{Ir} increases with increased electro-flocculation time and with IrO_2 nanoparticle concentration in the deposition solution. Remarkably, the current for water oxidation at +1.3 V varies nearly linearly over a >300-fold range of Γ_{Ir} of electroactive Ir^{V}/Ir^{IV} sites in the electro-deposited IrO_2 films. The films contain from sub- to multiple monolayers of the 1.6 nm nanoparticles (one monolayer is ~5×10^{-11} mol nanoparticles/cm^2). This important result means that, at a constant applied η, thicker IrO_x nanoparticle films can drive a proportionately more copious O_2 evolution without significant degradation of the Reaction (3.4) kinetics.

While possibly not all of the ca. 130 Ir sites/nanoparticle in the film are electroactive, the author has determined[18] that all sites are electroactive for 1.6 nm nanoparticles in pH 13 solutions. In experiments varying the quantity of electrodeposited IrO_x, the water oxidation current at 1.3 V vs. Ag/AgCl (pH 7.0, 1 M stirred phosphate buffer, after 150 sec.) was 91 mA/cm^2 (nearly 0.1 A/cm^2) for $\Gamma_{Ir} = 7\times10^{-8}$ mol/cm^2 of electroactive Ir^{V}/Ir^{IV} sites. This steady state current for water oxidation is ~40 times higher than previous (η

benchmark) reports[1,10] at the same potential. For small and large values of Γ_{Ir} ($< 2 \times 10^{-9}$, $\sim 6 \times 10^{-8}$ mol/cm^2),

the electroactive Ir site turnover rate (TO), during O_2 evolution was estimated from Figure 3.13 by

$$I_{cat} = nFAk_{cat}\Gamma_{Ir} \qquad (3.5)$$

as 6.0 and 4.5 s^{-1}, respectively. These TO results are similar to those of Yagi et al.[10] yet the present films

exhibit a substantially lowered η. An explanation must consider[2,8] how thick films of IrO$_x$ nanoparticles can

become, throughout, rapidly charged to the Ir^{VI} state and, throughout, react with water (Figure 3.13). Firstly,

electron conduction through the IrO$_x$ films must be very fast[11-13]. Perhaps more importantly, the exceptional

electrocatalytic reactivity of the electro-flocculated nanoparticle films may reflect a mesoporous structure, in

which the oxidation current density at IrO$_x$/electrolyte interfaces is kept at a reduced value by an extended
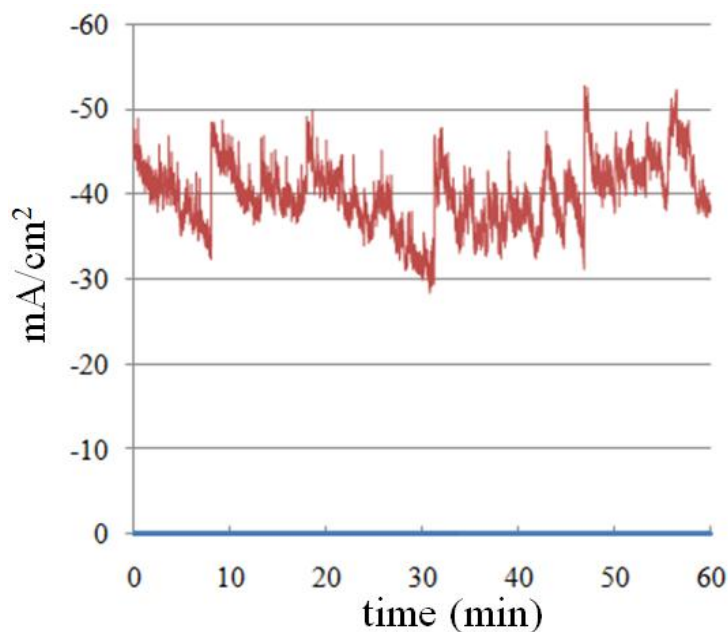
Figure 3.15. Stability of 1 hour current flow (red) during prolonged evolution of O_2 at a IrO$_x$ nanoparticle film-coated GC electrode, in 1.0 M phosphate buffer, with stirring, at pH 7. In comparison, current at bare GC is negligible (blue line).

internal surface area, irrespective of overall nanoparticle layer depth. That is, the nanoparticle films are

mesoporous, with facile water and ion permeation. Further experiments will be required to quantify this

hypothesis, but it is consistent with microscopy showing the highly porous character of the IrO$_x$ films (Figure

3.14). It is also noteworthy that the (1.6 nm) IrO_x employed here are much smaller than in the previous work.[10]

3.2.3 Oxygen detection using RRDE system

That the gas evolved from IrO_x films was O_2 derived from water oxidation was confirmed both by the in situ observation of an O_2 reduction peak at -0.4 V following potential excursion into the water oxidation wave, and by mass spectrometry of the gas electrolytically evolved from a pH 7 phosphate buffer containing 10 % $^{18}OH_2$. Applying a potential of +1.3 V vs. Ag/AgCl for 1 hr, with stirring, gave (Figure 3.15) a ~42 mA/cm^2 current (~8 ml/cm^{2}hr, 4×10^{-4} mol/cm^{2}hr, assuming 100% current efficiency). Mass spectrometry of the collected gas showed above background amounts of isotopically labelled $^{34}O_2$ and $^{36}O_2$ products.

The rotating ring disk electrode (RRDE) was used to more exactly quantify the current efficiency of O_2 production and to determine the potentials where 100% current efficiency was attained. The RRDE experiment is explained in Scheme 3.2, showing that O_2 evolved at the IrO_2 nanoparticle-coated GC disk electrode is hydrodynamically swept to the Pt ring electrode where it is detected by reduction to H_2O_2. The O_2 detection voltammetry is illustrated in Figure 3.16.

Collection Efficiency (%) (N/2) = $100 \times i_R/2i_D$
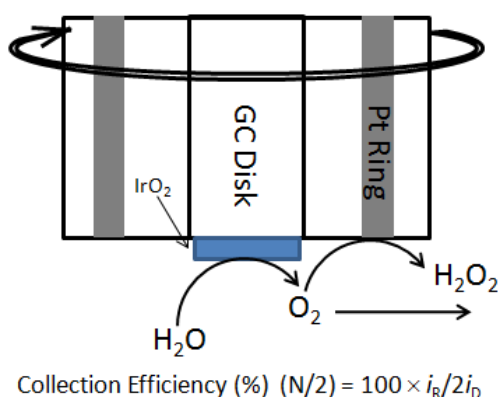
Scheme 3.2. RRDE detection at ring electrode, of O_2 generated from IrO_x coated glassy carbon disk electrode.   Calibrated collection efficiency N/2 is 19 % at pH 13 (See Figure 3.16).
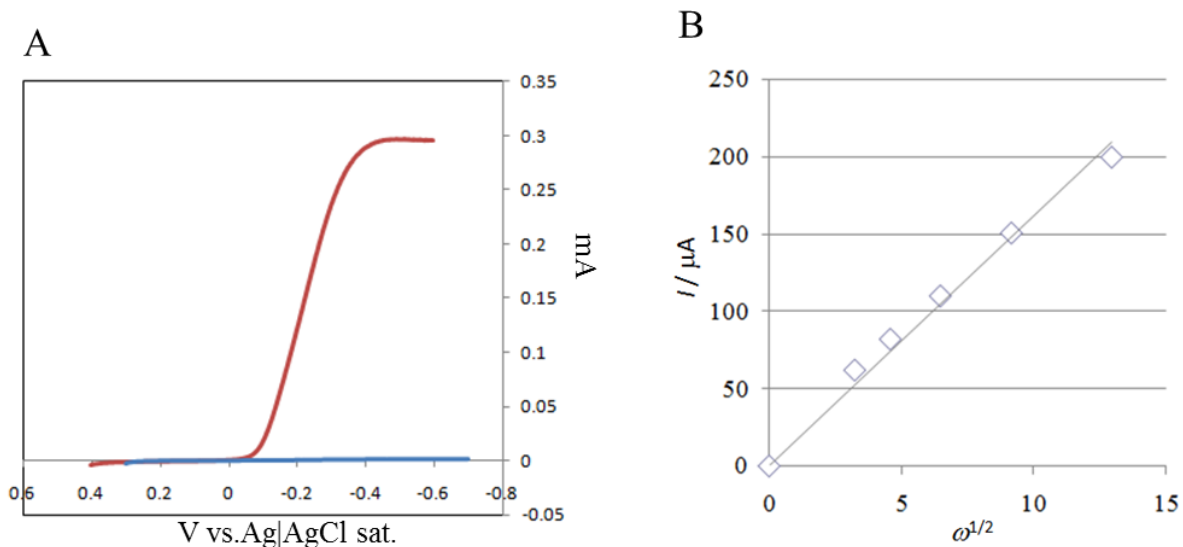
Figure 3.16. (A) Linear sweep voltammetry of platinum ring electrode with 1600 rpm in pH 13. Scan rate is 1 mVs^{-1}. Red line is air saturated condition, Blue line is argon saturated condition. (B) Levich plots of the current at -0.6 V in air saturated condition at pH 13 against rotation speed.
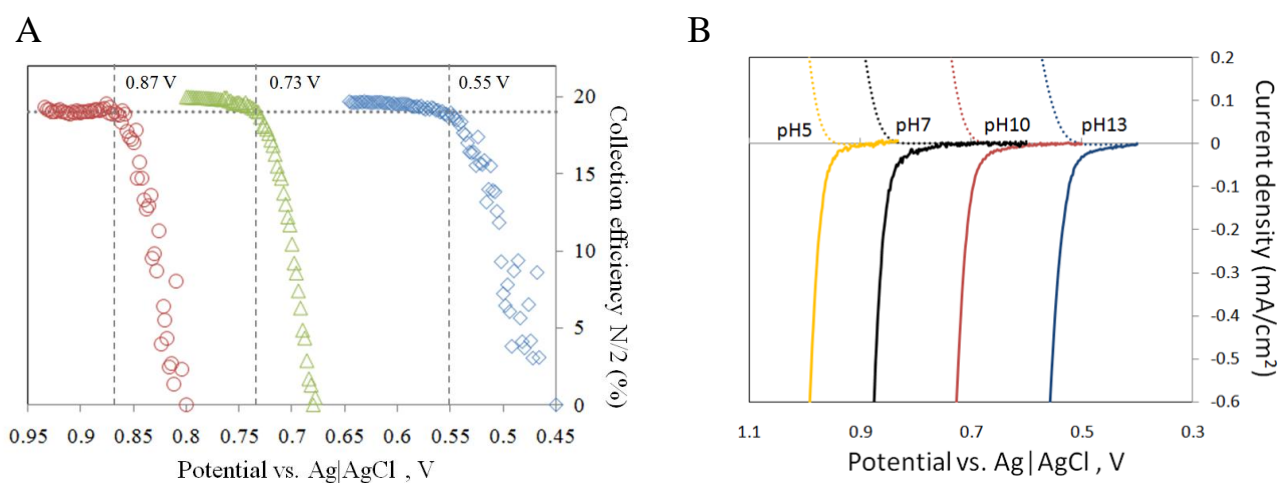
Figure 3.17. (A) RRDE collection efficiency $I_{RING}/2I_{DISK}$ = N/2 for O$_2$ evolution at pH 7 (red), 10 (ocher) and 13 (blue) with 1600 rpm in deaerated 1M phosphate. IrO$_x$ coated GC disk and Pt ring electrodes. Vertical dashed lines indicate N/2 = 19 %. Linear sweep voltammetry of water oxidation at IrOx coated glassy carbon disk electrode (lower solid curves), while detecting oxygen reduction at platinum ring disk electrode (upper dashed curves), at different pH solution. (B) Potential scan rate on GC disk electrode was 1 mV/s; potential of platinum ring electrode for detecting oxygen was constant at -0.6 V at pH 13, -0.5 V at pH 10 and -0.4 V at pH 7 and pH 5, respectively. Solutions of pH 10, 7 and 5 included 1 M NaH$_2$PO$_4$ with pH adjusted by NaOH. Γ_{Ir} = 3.5 × 10^{-8} mol/cm^2 on the disk electrode.
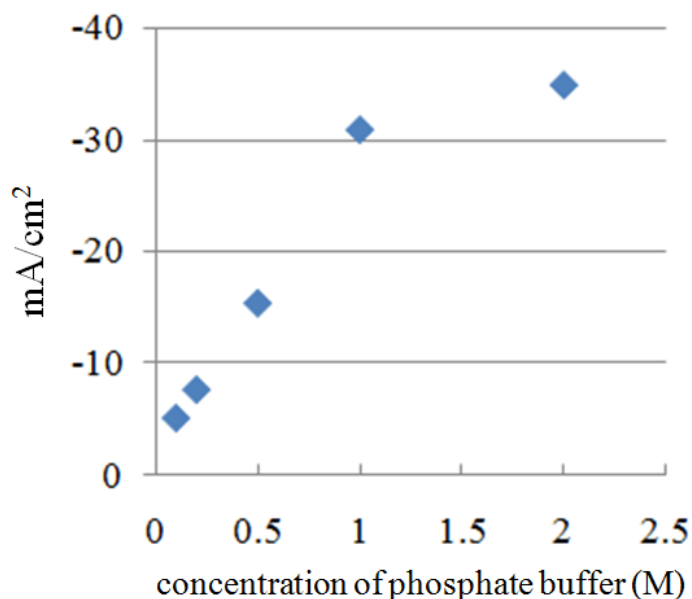
Figure 3.18. The electrocatalytic current density (after 150 s with stirring, at pH 7 and 1.3 V vs. Ag/AgCl) increases with the concentration of phosphate buffer. The effect is interpreted as countering the massive release of protons at the IrO_x film surface during water oxidation.

The I_{RING}/I_{DISK} collection efficiency (N) is a function solely of RRDE geometry and can thus be accurately calibrated. A factor of 2 accounts for the different numbers of electrons in the disk and ring reactions.

Figure 3.17 shows results for N/2 at three pH values. When N/2 = 19 %, current efficiency for O_2 generation at the IrO_2 nanoparticle-coated disk is 100 %; this is achieved at 0.55 V, 0.73 V and 0.87 V for pH 13, 10 and 7, respectively. These potentials correspond to an average $\eta \approx 0.25$ V, at a 0.5 mA/cm^2 disk current density. These results are almost identical to those from Figure 3.9 and are displayed in Figure 3.10B as blue circles. The actual onset of detectable O_2 evolution, when N/2 rises above ~ 0%, is seen in Figure 3.17 as 0.45V, 0.68V and 0.8V at pH 13, 10 and 7, respectively.

3.2.4. Conclusions

In conclusions, mesoporous films of 1.6 nm IrO_x nanoparticles can be electro-flocculated onto electrode surfaces like GC, Au, Pt, and ITO, in which the equivalent of ~10 monolayers of   electroactive

65

nanoparticles are active towards water oxidation. The electrocatalytic currents are large, ~0.1 A/cm^2 at +1.3V vs. Ag/AgCl at pH 7. The over-potential for oxygen evolution is small ($\eta \approx 0.25$V at 0.5 mA/cm^2, regardless of pH) and O$_2$ is evolved at 100% current efficiency at this over-potential. These impressive values may reflect a special chemistry of the 1.6 nm IrO$_x$ nanoparticles as well as the mesoporous structure's effect on the electrochemical current density.

3.2.5. Experimental

K$_2$IrCl$_6$ (99.99%) and NaH$_2$PO$_4$ (99%) were purchased from Aldrich and Sigma-Aldrich, respectively. Electrochemical measurements were carried out on a Bioanalytical Systems (BAS) 100B electrochemical analyzer. Electrodes were a BAS glassy carbon working electrode (dia. 3 mm), Pt flag counter electrode, and Ag/AgCl reference electrode. The working electrode was sometimes tilted to minimize occlusion by gas evolution. Modulated Speed electrode rotator was AFMSRCE and electrode was E7R9, from Pine Research Instrumentation, Inc.. The surface areas of glassy carbon disk and platinum ring electrodes are 0.259 and 0.185 cm^2, respectively. The water oxidation reaction on IrO$_x$ film involves four electrons while oxygen reduction on the Pt electrode involves two electrons, so the collection efficiency N is divided by two.   The collection efficiency of oxygen at pH 13 is 19 %, calibrated by Levich ring electrode equation and currents at applied -0.6 V on platinum ring electrode in air saturated solution. The IrO$_x$ adsorbed GC electrode was prepared as in text above. When detecting oxygen generated at the RRDE disk, oxygen was removed by bubbling Ar gas about 1 hour. Background current of platinum ring electrode at -0.6 V at 1600 rpm after deaerated is 100 times smaller than that of air saturated condition. TEM samples were prepared by placing a droplet containing IrO$_x$ nanoparticles onto a copper grid (200 copper mesh; carbon-coated Formvar). TEM images were obtained on a JEOL 2010F FasTEM electron microscope and scanning electron microscopy (SEM) images (Figure 3.14) on a Hitachi S-4700 FE-SEM.

3.3. Conclusions of section 3

In section 3.1, I describe the first example of redox catalysis using a dissolved electroactive nanoparticle, based on the oxidation of water by electro-generated IrO_X nanoparticles containing Ir^{VI} states, in pH 13 solutions of 1.6 ± 0.6 nm (dia.) $Ir^{IV}O_X$ nanoparticles capped solely by hydroxide. At potentials (ca. +0.45V) higher than the mass transport-controlled plateau of the nanoparticle $Ir^{V/IV}$ wave, rising large redox catalytic currents reflect electrochemical generation of Ir^{VI} states, which by +0.55 V and onwards to +1.0V are shown by rotating ring disk electrode experiments to lead with 100% current efficiency to the oxidation of water to O_2. O_2 production at +0.55V corresponds to an over-potential η of only 0.29 V, relative to thermodynamic expectations of the four electron $H_2O \rightarrow O_2$ reaction. The Ir site turnover frequency (TO, mol O_2/Ir sites/sec) is 8-11 s^{-1}.   Controlled potential coulometry shows that all Ir sites in these nanoparticles (average 66 Ir each) are electro-active, meaning that the nanoparticles are small enough to allow the required electron and proton transport throughout. Both the over-potential and TO values are nearly the same as observed previously for films electroflocculated from similar IrO_x nanoparticles, providing the first comparison of electrocatalysis by nanoparticle films with redox catalysis by dissolved, diffusing nanoparticles.

In section 3.2, I describe the formation of stable, adherent, mesoporous films of 1.6 nm dia. $Ir^{IV}O_x$ nanoparticles on glassy carbon electrodes, by a previously unreported method of controlled potential electro-flocculation from pH 13 nanoparticle solutions. These films initiate O_2 evolution from water oxidation and then achieve 100% current efficiency, at over-potentials only ~0.15 V and ~0.25 V higher, respectively, than the reversible H_2O/O_2 potential.   The over-potentials, measured at ~0.5 mA/cm^2, are independent of pH and are the smallest yet reported for electrochemical water oxidation, a property important in possible uses in electrochemical solar cells. The films appear to be mesoporous and microscopically accessible, since O_2 evolution currents increase proportionately to multi-layer nanoparticle film coverage but without concurrent increase in over-potential.

References and Notes

(1)   a) Kanan, M.W.; Nocera, D. G. Science 2008, 321, 1072. b) Surendranath, Y.; Dincă, M., Nocera, D.G. *J. Am. Chem. Soc*. **2009**, 131, 2615.

(2)   a) Morris, N. D.; Suzuki, M.; Mallouk, T. E. *J. Phys. Chem. A* **2004**, 108, 9115. b) Hoertz, P. G.; Kim, Y.; Youngblood, W. J.; Mallouk, T. E.;   *J. Phys. Chem. B* **2007**, 111, 6845.   c)   Youngblood, W.J.; Lee, S-H.A.; Kobayashi, Y.; Hernandez-Pagan, E.A.; Hoertz, P.G.; Moore, T.A.; Moore, A.L.; Gust, D. and Mallouk, T.E.   *J. Am. Chem. Soc.* **2009**, 131, 926-927.

(3)   O'Regan, B.; Gräetzel, M. *Nature* **1991**, 353, 737.

(4)   a) Gersten, S. W.; Samuels, G. J.; Meyer, T. J. *J. Am. Chem. Soc.* **1982**, 104, 4029. b) Concepcion, J. J.; Jurss, J. W.; Templeton, J. L.; Meyer, T. J. *Proc. Nat. Acad. Sci., U. S.*   **2008**, 105, 17632.

(5)   McDaniel, N. D.; Coughlin, F. J.; Tinker, L. L; Bernhard, S. *J. Am. Chem. Soc. 2008*, **130**, 210.

(6)   Zong, R.; Thummel, R. P.; *J. Am. Chem. Soc.* **2005**, 127, 12802.

(7)   Geletii, Y. V.; Botar, B.; Kögerler, P.; Hillesheim, D. A.; Musaev, D. G.; Hill, C. L. . *Angew. Chem. Int. Ed.* **2008**, 47, 3896.

(8)   a) Harriman, A.; Pickering, I. J.; Thomas, J. M.; Christensen, P. A. *J. Chem. Soc., Faraday Trans. 1* **1988**, 84, 2795. b) Harriman, A.; Thomas, J. M.; Millward, G. R. New. J. Chem. 1987, 11, 757.

(9)   a) Kiwi, J.; Graetzel, M. *Angew. Chem., Int. Ed. Engl.* **1978**, 17, 860. b) Kiwi, J.; Graetzel, M. *Angew. Chem., Int. Ed. Engl.* **1979**, 18, 624.

(10)   a) Yagi, M.; Tomita, E.; Sakita, S.; Kuwabara, T.; Nagai, K. *J. Phys. Chem. B* **2005**, 109, 21489. b) Kuwabara, T.; Tomita, E.; Sakita, S.; Hasegawa, D.; Sone, K.; Yagi, M. *J. Phys. Chem. C* **2008**, 112, 3774-3779

(11)   Petit, M. A.; Plichon, V. *J. Electroanal. Chem.* **1998**, 444, 247.

(12)   Brewer, S.H.; Wicaksana, D.; Maria, J-P.; Kingon, A. I.; Franzwz, S. *Chem. Phys.* **2005**, 313, 25.

(13)   Chen, Y.; Shi, P.; Scherson, D. *Electrochemical and Solid-State Letters*. **2008**, 11, F5

(14)   Comninellis, Ch.; Vercesi, G. P. *J. Appl. Electrochem.* **1991**, 21, 335.

(15)   a)   Following Wohler,15b 2.4 mM aqueous K_2IrCl_6 was adjusted to pH 13 with conc. NaOH, heated at $90^{\circ}C$ for 20 min, and immediately cooled in an ice-bath, producing a blue solution (optical absorbance peak at 582 nm, indicating[4,10] $Ir^{IV}O_x$) containing well dispersed, stable 1.6 nm dia. nanoparticles that remained unchanged for >2 months at pH 13 in a refrigerator. b) Wohler, L.; Witzmann, W. Z. *Anorg. Chem.* **1908**, 57, 323.

(16)   Nakagawa, T.; Murray, R. W. unpublished data, Univ. No. Car. 2009.

(17)   a) Accurately observing the pH dependence required a high buffer capacity (1 M phosphate as opposed to 0.1 M) owing to the large rate of water oxidation and consequent surface proton release (see Figure 3.18). b) At a bare GC electrode in 1 M pH 7 phosphate buffer, water oxidation begins at ~1.6 V vs. Ag/AgCl.

(18)   Nakagawa, T.; Bjorge, N.; Murray, R. W. *J. Am. Chem. Soc.* **2009**, 131 (43), 15578–15579

4. Conclusions

In this article, the author has reported the development of functional electrodes for realizing efficient electrochemical catalytic redox reactions of oxygen/water under neutral conditions and ambient temperature. To realize a highly efficient functional electrode, some factors need to considered; some of these factors are high activity of the catalyst, carrying out a modified method on the electrode surface while maintaining the catalyst activity, a porous electrode with a large surface area, maintaining a continuous supply of substrate, electron transfer between electrode and catalyst, and high electron conductivity of a porous electrode.

In section 2, the fabrication of an enzyme-modified electrode via the production of diffusion-limited bioelectrocatalytic current for the reduction of O_2 to water at neutral pH and at ambient temperature has been reported. The electrode uses bilirubin oxidase as an enzyme and $[Fe(CN)_6]^{3-/4-}$ as a mediator, both of which are immobilized on the surface of a glassy carbon electrode by electrostatic entrapment with poly-L-lysine. This modified method can be applied on carbon fiber electrodes that have a large surface area. The catalytic current density of a BOD-$[W(CN)_8]^{3-/4-}$-PLL CF fixed disk electrode is about 20–30 mA/cm^2 at 2000 rpm under oxygen-saturated conditions. In order to use this CF electrode in a biofuel cell for practical use, sufficient supply of oxygen and protons is required unless oxygen gas flow and a pump system are employed. Water repellents (Scotchgard^{TM}) dissolved in methyl isobutyl ketone are directly applied to this CF electrode after immobilization of an enzyme and a mediator. Sufficient oxygen and protons can be supplied to the BOD-$[Fe(CN)_6]^{3-/4-}$-PLL CF electrode in a concentrated buffer even under passive conditions, and an oxygen reduction current increased up to 24 mA/cm^2 at 0 V vs. Ag/AgCl under an air atmosphere, neutral pH and ambient temperature. The power density of a biofuel cell using this novel biocathode can reach up to 10 mW/cm^2; this power is sufficient to drive 100-mW portable music players with a stuck cell. The achievement of this magnitude of power density is a current world record, and this result may be a big step toward realizing practical uses of biofuel cells. The author is of the view that the research presented herein can be applied to any enzyme-modified electrode in order to increase its efficiency.

Section 3 presents the first example of redox catalysis performed using a dissolved electroactive nanoparticle; this catalysis is based on the oxidation of water by electrogenerated $Ir^{IV}O_X$ nanoparticles,

capped solely by hydroxides and having a diameter of 1.6 ± 0.6 nm, in solutions of pH 13. The results of controlled potential coulometry show that all Ir sites on these nanoparticles (average of 66 Ir atoms (sites) on each nanoparticles) are electroactive, indicating that the nanoparticles are small enough to allow the required electron and proton transport throughout, although only 3.7% and 16% of IrO_x is electroactive at the planar electrode and film aggregated 50–100 nm IrO_2 nanoparticles, respectively. Mesoporous films of 1.6 nm IrO_x nanoparticles can be electroflocculated onto electrode surfaces such as those of GC, Au, Pt, and ITO, in which the equivalent of ~10 monolayers of electroactive nanoparticles are active toward water oxidation. The electrocatalytic currents are large—i.e., ~0.1 A/cm^2 at +1.3 V vs. Ag/AgCl at pH 7—although the maximum value of such currents is 3 mA/cm^2 in an ITO electrode with modified 50–100 nm IrO_2 nanoparticles. Further, a simple oxygen detection method based on an RRDE measurement system has also been described; this analysis method is expected to be useful for the investigation of water splitting.

4. List of publications

1. <u>Nakagawa, T.</u>; Tsujimura, S.; Kano, K.; Ikeda, T. "Bilirubin Oxidase and $[Fe(CN)_6]^{3-/4-}$ Modified Electrode Allowing Diffusion-controlled Reduction of O_2 to Water at pH 7.0", *Chemistry Letters*, **2003**, 32 (1), pp 54-55.

2. <u>Nakagawa, T.</u>; Beasley, C. A.; Murray, R. W. "Efficient Electro-Oxidation of Water near Its Reversible Potential by a Mesoporous IrOx Nanoparticle Film", *Journal of Physical Chemistry C*, **2009,** 113 (30), pp 12958–12961.

3. <u>Nakagawa, T.</u>; Bjorge, N. S.; Murray, R. W. "Electrogenerated IrOx Nanoparticles as Dissolved Redox Catalysts for Water Oxidation", *Journal of American Chemical Society*, **2009**, 131 (43), pp 15578–15579.

4. <u>Nakagawa, T.</u>; Mita, H.; Kumita, H.; Sakai, H.; Tokita, Y.; Tsujimura, S. "Water-repellent-treated enzymatic electrode for passive air-breathing biocathodic reduction of oxygen", *Electrochemistry Communications*, **2013**, (36), pp 46-49.

5. Tsujimura, S.; Kawaharada, M.: <u>Nakagawa, T.</u>: Kano, K.:Ikeda, T. "Mediated bioelectrocatalytic O_2 reduction to water at highly positive electrode potentials near neutral pH", *Electrochemistry Communications*, **2003**, 5 (2), pp 138-141.

6. Tsujimura, S.; <u>Nakagawa, T.</u>; Kano, K; Ikeda, T. *Electrochemistry,* **2004**, 72, (6) pp 437-439.

7. Sakai, H.; <u>Nakagawa, T.</u>; Tokita, Y.; Hatazawa, T.; Ikeda, T.; Tsujimura, S.: Kano, K. "A high-power glucose/oxygen biofuel cell operating under quiescent conditions", *Energy & Environmental Science,* **2009**, 2, pp 133-138.

5. Acknowledgement